Symmetries in zero and finite center-of-mass momenta excitons

Robin Bajaj[1], Namana Venkatareddy[1], H. R. Krishnamurthy[1,2] and Manish Jain[1*]

[1] *Centre for Condensed Matter Theory, Department of Physics, Indian Institute of Science, Bangalore 560012, India and*

[2] *International Centre for Theoretical Sciences, Tata Institute of Fundamental Research, Bengaluru 560089, India*

(Dated: August 25, 2025)

Abstract

We present a symmetry-based framework for the analysis of excitonic states, incorporating both time-reversal and space-group symmetries. We demonstrate the use of time-reversal and space-group symmetries to obtain exciton eigenstates at symmetry-related center-of-mass momenta in the entire Brillouin zone from eigenstates calculated for center-of-mass momenta in the irreducible Brillouin zone. Furthermore, by explicitly calculating the irreducible representations of the little groups, we classify excitons according to their symmetry properties across the Brillouin zone. Using projection operators, we construct symmetry-adapted linear combinations of electron–hole product states, which block-diagonalize the Bethe–Salpeter Equation (BSE) Hamiltonian at both zero and finite exciton center-of-mass momenta. This enables a transparent organization of excitonic states and provides direct access to their degeneracies, selection rules, and symmetry-protected features. As a demonstration, we apply this formalism to monolayer MoS_2, where the classification of excitonic irreducible representations and the block structure of the BSE Hamiltonian show excellent agreement with compatibility relations derived from group theory. Beyond this material-specific example, the framework offers a general and conceptually rigorous approach to the symmetry classification of excitons, enabling significant reductions in computational cost for optical spectra, exciton–phonon interactions, and excitonic band structure calculations across a wide range of materials.

I. INTRODUCTION

Symmetry principles lie at the heart of quantum physics, governing both fundamental laws and emergent phenomena. In quantum systems, the transformation properties of energy eigenstates under symmetry operations [1–4] dictate degeneracies, selection rules, and responses to external perturbations. In electronic structure calculations, for instance, Bloch's theorem provides a powerful simplification by exploiting the lattice periodicity, restricting calculations to momenta within the first Brillouin zone (BZ). Additionally, space group symmetries allow for further computational efficiency by identifying symmetry-equivalent points in the BZ, reducing the sampling space and enabling the classification of eigenstates into

* mjain@iisc.ac.in

irreducible representations. These group-theoretical techniques are routinely employed in both one-electron and lattice dynamical problems to streamline band structure calculations and enforce optical selection rules.

In one-electron as well as phonon band structures, eigenstates at a given point in the BZ are routinely labeled by the irreducible representations of the little group at that point giving the symmetry classification of first-principles wavefunctions [2–4]. These symmetry-based insights are now deeply integrated into modern electronic structure workflows, providing both conceptual guidance and computational gains across condensed matter theory. Tools such as the Bilbao Crystallographic Server [5], SPGREP package [6] and IRREP package [7] enable block-diagonalization of Hamiltonians, degeneracy classification, and compatibility relation tracking capabilities that are now central to high-throughput and symmetry-aware materials discovery.

Despite their success in one-electron and phonon problems, such symmetry-based approaches remain underutilized in the context of excitons. Excitons feature prominently in the optical response of semiconductors and insulators, and are particularly well described within the Bethe–Salpeter equation (BSE) formalism [8–11]. The eigenstates of the BSE Hamiltonian, being two-particle bound states labeled by their center-of-mass (COM) momenta and dependent on relative momenta, differ from one-electron eigenstates in terms of the structure and the application of symmetry operations. Recently, some studies have addressed the role of symmetry in excitons. For example, Ref. [12] analyzes the excitonic band structure of monolayer MoS_2 and interprets the symmetry of low-lying excitons using group theory. Ref. [13] reports measurements of the exciton fine structure in monolayer MoS_2, highlightling the irreducible representations of two optically active (bright) excitons with parallel spins, along with two spin-forbidden dark states. Galvani *et al.* [14] investigate the symmetry properties of excitons in a monolayer hBN by combining *ab-initio* calculations with a tight-binding Wannier analysis in both real and reciprocal space. Similarly, Ref. [15] examines the influence of uniaxial strain on the symmetry classification of excitons in C_3N, employing a tight-binding BSE framework. In another work focused on excitonic g-factors in monolayer WSe_2 [16], the low-energy excitons are classified by tracking the compatibility relations between the little group C_{3v} at the K/K' points and the full point group D_{3h} at the Γ point. While these studies provide valuable insights at specific high-symmetry points, a systematic symmetry-based classification of the eigenstates of the BSE across the Brillouin zone within an *ab initio* framework is still largely unexplored.

In addition to providing insight and understanding, symmetries can be used to reduce the computational cost of the calculations. In the context of one-electron states, most widely used electronic structure codes, such as VASP [17], QUANTUMESPRESSO [18], and ABINIT [19], routinely incorporate symmetry-based optimizations to reduce computational cost and ensure physically meaningful results. This is used by calculating the electronic states for momenta within the irreducible part of the BZ and using symmetry to transform them to states with momenta within the rest of the BZ. Furthermore, in the context of lattice dynamics, similar symmetry-based approaches are used. Codes such as PHONOPY [20] and PHONO3PY [21] leverage crystal symmetries to reduce the cost of calculating dynamical matrices. However, similar ideas to use symmetry to reduce the computational costs in problems where excitons at finite COM are essential have not yet been employed. Many important physical phenomena such as exciton-phonon scattering [22–27], indirect optical transitions [24], and exciton thermalization dynamics [28] require detailed knowledge of excitonic states for a dense COM momentum-grid. Exciton-phonon coupling, in particular, determines linewidths and exciton thermalisation dynamics [28]. In systems like MoS_2 [22, 29], achieving convergence of calculations of the optical spectra demands fine sampling of the COM momenta in the BZ, especially near band extrema where small momentum shifts can strongly modulate coupling strength. Similarly, modeling exciton dynamics via the Boltzmann equation [28] and indirect optical spectra calculations in hBN, silicon, and bilayer MoS_2 [24, 30–33] require extensive sampling of finite COM momenta excitonic states. However, performing BSE calculations across such fine COM momenta meshes is computationally prohibitive for most materials. This further underscores the need for a symmetry-adapted approach to excitons that is grounded in an *ab initio* framework.

In this work, we develop a comprehensive symmetry-based formalism for exciton calculations within an *ab initio* framework. By applying space group operations on exciton wavefunctions at finite COM momentum, $\mathbf{Q}$, we reconstruct the wavefunctions for momenta in the full BZ from computations for $\mathbf{Q}$ restricted to the irreducible wedge. We further classify excitonic eigenstates into irreducible representations, providing a rigorous symmetry-resolved picture of exciton physics. At $\mathbf{Q} = 0$, we use symmetry-adapted bases to block-diagonalize the BSE Hamiltonian, reducing both diagonalization time and memory usage.

By systematically incorporating crystal symmetry into excitonic theory, our approach delivers both conceptual and computational advances. It enables scalable BSE calculations for complex systems and provides a robust foundation for interpreting exciton phenomena through the lens of symmetry.

II. THEORETICAL FORMALISM

A. Preliminaries: Space group symmetries and time-reversal symmetry in one-electron wavefunctions

In periodic solids, the translational symmetry of the lattice ensures that the one-electron Hamiltonian $\hat{\mathcal{H}}$ commutes with the lattice translation operator, $\hat{T}_{\mathbf{R}}$, where $\mathbf{R}$ is a Bravais lattice vector. As a result, $\hat{\mathcal{H}}$ can be written as a direct sum of independent Hamiltonians at each crystal momentum $\mathbf{k}$ in the Brillouin zone,

$$\hat{\mathcal{H}} = \bigoplus_{\mathbf{k}} \mathcal{H}_{\mathbf{k}} \tag{1}$$

This block-diagonal structure implies that the wavefunctions can be chosen to be eigenstates of the translation operators, leading to the Bloch form

$$\psi_{n,\mathbf{k}}(\mathbf{r}) = e^{i\mathbf{k}\cdot\mathbf{r}}\, u_{n,\mathbf{k}}(\mathbf{r}) \tag{2}$$

where $u_{n,\mathbf{k}}(\mathbf{r})$ is periodic with the lattice. The cell periodic part $u_{n,\mathbf{k}}(\mathbf{r})$ is commonly expanded in a plane-wave basis as:

$$u_{n,\mathbf{k}}(\mathbf{r}) = \sum_{\mathbf{G}} c_{n,\mathbf{k}}(\mathbf{G}) e^{i\mathbf{G}\cdot\mathbf{r}} \tag{3}$$

where $\mathbf{G}$ are reciprocal lattice vectors and $c_{n,\mathbf{k}}(\mathbf{G})$ are the expansion coefficients. This representation naturally incorporates translational symmetry and facilitates the treatment of additional crystal symmetries.

The symmetry properties of Bloch wavefunctions are central to understanding electronic band structures and the selection rules governing optical transitions. Due to the space-group symmetry of the underlying crystal lattice, Bloch wavefunctions are constrained to transform in specific ways under the corresponding symmetry operations. These transformations determine the irreducible representations associated with the wavefunctions.

Let $\hat{P}_{\{\mathcal{R}_\mathbf{t}\,|\,\mathbf{t}\}}$ represent a symmetry operator associated with $\{\mathcal{R}_\mathbf{t}\,|\,\mathbf{t}\} \in \mathcal{G}$, where $\mathcal{R}_\mathbf{t}$ denotes a point-group operation (such as rotation, mirror reflection, or inversion), $\mathbf{t}$ is a fractional translation, and $\mathcal{G}$ is the crystal space group. Due to the underlying symmetry of the lattice, $\hat{P}_{\{\mathcal{R}_\mathbf{t}\,|\,\mathbf{t}\}}$ commutes with the Hamiltonian, $[\hat{P}_{\{\mathcal{R}_\mathbf{t}\,|\,\mathbf{t}\}}, \hat{\mathcal{H}}] = 0$. $\hat{P}_{\{\mathcal{R}_\mathbf{t}\,|\,\mathbf{t}\}}$ maps $\mathcal{H}_\mathbf{k}$ to $\mathcal{H}_{\mathcal{R}_\mathbf{t}\mathbf{k}}$ via $\mathcal{H}_{\mathcal{R}_\mathbf{t}\mathbf{k}} = \hat{P}^{-1}_{\{\mathcal{R}_\mathbf{t}\,|\,\mathbf{t}\}}\,\mathcal{H}_\mathbf{k}\,\hat{P}_{\{\mathcal{R}_\mathbf{t}\,|\,\mathbf{t}\}}$. This implies that if a wavevector $\mathbf{k}$ is mapped to $\mathcal{R}_\mathbf{t}\mathbf{k}$ by a symmetry operation, the energy eigenvalues corresponding to $\mathbf{k}$ and $\mathcal{R}_\mathbf{t}\mathbf{k}$ remain same *i.e.* $\epsilon_{n,\mathcal{R}_\mathbf{t}\mathbf{k}} = \epsilon_{n,\mathbf{k}}$. The action of the symmetry operator on the Bloch wavefunction transforms it according to

$$\hat{P}_{\{\mathcal{R}_\mathbf{t}\,|\,\mathbf{t}\}}\,\psi_{n,\mathbf{k}}(\mathbf{r}) = \psi_{n,\mathbf{k}}\left(\mathcal{R}_\mathbf{t}^{-1}(\mathbf{r}-\mathbf{t})\right) \tag{4}$$

Utilizing Bloch's form as defined in Eq. 2, the transformation becomes:

$$\hat{P}_{\{\mathcal{R}_\mathbf{t}|\mathbf{t}\}}\psi_{n,\mathbf{k}}(\mathbf{r}) = u_{n,\mathcal{R}_\mathbf{t}\mathbf{k}}(\mathbf{r})e^{i\mathcal{R}_\mathbf{t}\mathbf{k}.(\mathbf{r}-\mathbf{t})} \tag{5}$$

The cell-periodic function $u_{n,\mathcal{R}_\mathbf{t}\mathbf{k}}(\mathbf{r}) = u_{n,\mathbf{k}}(\mathcal{R}_\mathbf{t}^{-1}(\mathbf{r}-\mathbf{t}))$ and can be written as:

$$u_{n,\mathcal{R}_\mathbf{t}\mathbf{k}}(\mathbf{r}) = \sum_\mathbf{G} c_{n,\mathbf{k}}(\mathcal{R}_\mathbf{t}^{-1}\mathbf{G})e^{-i\mathbf{G}\cdot\mathbf{t}}e^{i\mathbf{G}\cdot\mathbf{r}} \tag{6}$$

Substituting this into Eq. 5 yields the transformation rule for the plane-wave coefficients at $\mathcal{R}_\mathbf{t}\mathbf{k}$ in terms of those at $\mathbf{k}$:

$$c_{n,\mathcal{R}_\mathbf{t}\mathbf{k}}(\mathbf{G}) = c_{n,\mathbf{k}}(\mathcal{R}_\mathbf{t}^{-1}\mathbf{G})e^{-i(\mathbf{G}+\mathcal{R}_\mathbf{t}\mathbf{k})\cdot\mathbf{t}} \tag{7}$$

This equation captures how the plane-wave components of the Bloch wavefunction transform under a space group operation. In systems without degeneracy and spin, this relation uniquely determines the coefficients at $\mathcal{R}_\mathbf{t}\mathbf{k}$, up to a common phase factor across all bands.

When spin degrees of freedom are included, the symmetry properties of Bloch wavefunctions must account for both spatial transformations and their induced effects on spinors. Although lattice symmetries act on spatial coordinates in $\mathbb{R}^3$, they also act on the spin degrees of freedom, which transform under SU(2), the double cover of the spatial rotation group SO(3).

A spinor Bloch wavefunction can be expressed as a two-component column vector:

$$\Psi_{n,\mathbf{k}}(\mathbf{r}) = \begin{bmatrix} \psi_{n,\mathbf{k},\uparrow}(\mathbf{r}) \\ \psi_{n,\mathbf{k},\downarrow}(\mathbf{r}) \end{bmatrix} = \begin{bmatrix} u_{n,\mathbf{k},\uparrow}(\mathbf{r})e^{i\mathbf{k}\cdot\mathbf{r}} \\ u_{n,\mathbf{k},\downarrow}(\mathbf{r})e^{i\mathbf{k}\cdot\mathbf{r}} \end{bmatrix} \tag{8}$$

where $u_{n,\mathbf{k},\sigma}(\mathbf{r})$ are periodic functions and $\sigma =\uparrow,\downarrow$ denotes the spin index.

A general symmetry operation involving spin can be written as the direct product of a spatial operation and a corresponding spinor transformation:

$$\hat{P}^{sp}_{\{\mathcal{R}_{\mathbf{t}}|\mathbf{t}\}} = \hat{P}_{\{\mathcal{R}_{\mathbf{t}}|\mathbf{t}\}} \otimes \hat{\mathcal{T}}_{\mathcal{R}_{\mathbf{t}}} \tag{9}$$

where $\hat{P}^{sp}_{\{\mathcal{R}_{\mathbf{t}}|\mathbf{t}\}}$ denotes the full operator that corresponds to the symmetry operation $\{\mathcal{R}_{\mathbf{t}}|\mathbf{t}\}$, $\hat{P}_{\{\mathcal{R}_{\mathbf{t}}|\mathbf{t}\}}$ and $\hat{\mathcal{T}}_{\mathcal{R}_{\mathbf{t}}}$ denote its spatial and spin components, respectively. The dependence on $\mathbf{t}$ is dropped from $\hat{\mathcal{T}}_{\mathcal{R}_{\mathbf{t}}}$ since fractional translations do not affect the spinor representation. Let $\mathcal{T}^{\sigma,\sigma'}_{\mathcal{R}_{\mathbf{t}}}$ be the matrix elements of the SU(2) representation corresponding to $\hat{\mathcal{T}}_{\mathcal{R}_{\mathbf{t}}}$. Since spinors transform under the SU(2) representation of rotations, their behavior is governed by the homomorphism between SO(3) and SU(2), given by:

$$\mathcal{T} : \mathrm{SO}(3) \to \mathrm{SU}(2) \tag{10}$$

This mapping is a two-to-one covering: each rotation $\mathcal{R}_{\mathbf{t}} \in \mathrm{SO}(3)$ corresponds to two elements $\pm\mathcal{T}_{\mathcal{R}_{\mathbf{t}}} \in \mathrm{SU}(2)$. Consequently, under a full 2π rotation, a spinor acquires a phase of -1, reflecting the half-integer spin of electrons.

The action of the full symmetry operator $\hat{P}^{sp}_{\{\mathcal{R}_{\mathbf{t}}|\mathbf{t}\}}$ on the spinor Bloch wavefunction $\Psi_{n,\mathbf{k}}(\mathbf{r})$ is:

$$\hat{P}^{sp}_{\{\mathcal{R}_{\mathbf{t}}|\mathbf{t}\}} \Psi_{n,\mathbf{k}}(\mathbf{r}) = \sum_{\sigma'} \mathcal{T}^{\sigma,\sigma'}_{\mathcal{R}_{\mathbf{t}}} \psi_{n,\mathcal{R}_{\mathbf{t}}\mathbf{k},\sigma'}(\mathbf{r}) \tag{11}$$

The explicit form of the SU(2) spinor matrix for a rotation by an angle, θ, about the $\hat{n}$ axis:

$$\mathcal{T}^{\sigma,\sigma'}_{\mathcal{R}_{\mathbf{t}}} = \begin{bmatrix} \cos\left(\frac{\theta}{2}\right) - in_z \sin\left(\frac{\theta}{2}\right) & (-n_y - in_x)\sin\left(\frac{\theta}{2}\right) \\ (n_y - in_x)\sin\left(\frac{\theta}{2}\right) & \cos\left(\frac{\theta}{2}\right) + in_z \sin\left(\frac{\theta}{2}\right) \end{bmatrix} \tag{12}$$

This unitary transformation guarantees that the spinors are transformed correctly under spatial rotations. For a general rotation, the directions $\hat{n} = (n_x, n_y, n_z)$ and θ are chosen based on $\mathcal{R}_{\mathbf{t}}$. Because $\mathcal{T}_{\mathcal{R}_{\mathbf{t}}} \in \mathrm{SU}(2)$, spinor wavefunctions obey a different transformation law from scalar wavefunctions. This leads to the emergence of half-integer representations and the necessity to use double groups with distinct irreducible representations.

A key consequence of the SU(2)-SO(3) homomorphism is the sign ambiguity in group multiplication. If two spatial rotations $(\mathcal{R}_{\mathbf{t}})_i$ and $(\mathcal{R}_{\mathbf{t}})_j$ combine to form $(\mathcal{R}_{\mathbf{t}})_k$, that is,

$$(\mathcal{R}_{\mathbf{t}})_i(\mathcal{R}_{\mathbf{t}})_j = (\mathcal{R}_{\mathbf{t}})_k \tag{13}$$

Then their corresponding spin representations satisfy:

$$(\mathcal{T}_{\mathcal{R}_{\mathbf{t}}})_i(\mathcal{T}_{\mathcal{R}_{\mathbf{t}}})_j = \pm(\mathcal{T}_{\mathcal{R}_{\mathbf{t}}})_k \tag{14}$$

The additional sign arises from the double cover nature of SU(2) over SO(3). Specifically, a 2π rotation changes the sign of a spinor wavefunction, a fundamental property underlying fermionic statistics, and the behavior of electrons in systems with spin-orbit coupling. This sign ambiguity is reflected in the group multiplication rules of double groups, where the symmetry elements remain the same, but the signs depend on the chosen branch of the SU(2) representation corresponding to a given SO(3) rotation.

So far, our discussion has been restricted to cases where the energy eigenstates are non-degenerate, both with and without spin-orbit coupling. However, the presence of degeneracies introduces an additional complexity in the symmetry analysis, since multiple wave functions may mix under the action of symmetry operations. Under a symmetry operation $\mathcal{R}_{\mathbf{t}}$, a Bloch state $|\psi_{m\mathbf{k}}\rangle$ can transform into a linear combination of states within the degenerate manifold. This transformation can be written as:

$$\hat{P}_{\{\mathcal{R}_{\mathbf{t}}|\mathbf{t}\}}|m,\mathbf{k}\rangle = \sum_{n} \mathcal{D}^{n,m}_{\mathcal{R}_{\mathbf{t}}\mathbf{k}}(\{\mathcal{R}_{\mathbf{t}}|\mathbf{t}\})|n,\mathcal{R}_{\mathbf{t}}\mathbf{k}\rangle \tag{15}$$

From this point onward, we use the simplified notation $|n,\mathbf{k}\rangle$ to represent one-particle Bloch states. The coefficients $\mathcal{D}^{n,m}_{\mathcal{R}_{\mathbf{t}}\mathbf{k}}(\{\mathcal{R}_{\mathbf{t}}|\mathbf{t}\})$ define a unitary transformation matrix associated with the symmetry operation $\{\mathcal{R}_{\mathbf{t}}|\mathbf{t}\}$ within the degenerate subspace. These elements are obtained from the overlap between the rotated wavefunctions and the original states:

$$\mathcal{D}^{n,m}_{\mathcal{R}_{\mathbf{t}}\mathbf{k}}(\{\mathcal{R}_{\mathbf{t}}|\mathbf{t}\}) = \langle n,\mathcal{R}_{\mathbf{t}}\mathbf{k}|\hat{P}_{\{\mathcal{R}_{\mathbf{t}}|\mathbf{t}\}}|m,\mathbf{k}\rangle \tag{16}$$

A particularly important case arises when $\{\mathcal{R}_{\mathbf{t}}|\mathbf{t}\} \in \mathcal{G}_{\mathbf{k}}$, where $\mathcal{G}_{\mathbf{k}}$ denotes the little group of the wavevector $\mathbf{k}$, i.e., the subset of the space group symmetry operations that leave $\mathbf{k}$ invariant modulo a reciprocal lattice vector $\mathbf{G}$, such that $\mathcal{R}_{\mathbf{t}}\mathbf{k} = \mathbf{k} \pm \mathbf{G}$. In this case, the transformation reduces to:

$$\mathcal{D}^{n,m}_{\mathcal{R}_{\mathbf{t}}\mathbf{k}}(\{\mathcal{R}_{\mathbf{t}}|\mathbf{t}\}) = \langle n,\mathbf{k}|\hat{P}_{\{\mathcal{R}_{\mathbf{t}}|\mathbf{t}\}}|m,\mathbf{k}\rangle = U^{n,m}_{\mathbf{k}}(\{\mathcal{R}_{\mathbf{t}}|\mathbf{t}\}), \tag{17}$$

where $U^{n,m}_{\mathbf{k}}(\{\mathcal{R}_{\mathbf{t}}|\mathbf{t}\})$ corresponds to an irreducible representation of the symmetry $\{\mathcal{R}_{\mathbf{t}}|\mathbf{t}\}$ within the little group $\mathcal{G}_{\mathbf{k}}$. This result implies that, in the presence of degeneracies, symmetry operations act within the degenerate subspace according to irreducible representations of the little group.

For non-degenerate states, the symmetry representation simplifies to a one-dimensional character $e^{i\theta}$, reflecting the fact that the wavefunction transforms into itself up to a complex phase under $\{\mathcal{R}_{\mathbf{t}}|\mathbf{t}\}$. In contrast, for an n-fold degenerate manifold, arising, for instance, due to spin, crystal symmetries, or fundamental symmetries such as time-reversal, the representation becomes n-dimensional. These higher-dimensional irreducible representations determine the structure of degeneracies in the band structure and restrict the allowed symmetry-adapted basis states.

In the case of non-spinor wavefunctions (i.e., in the absence of spin-orbit coupling), the irreducible representation of the symmetry operation $\{\mathcal{R}_{\mathbf{t}}|\mathbf{t}\}$ takes the form:

$$U^{m,n}_{\mathbf{k}}(\{\mathcal{R}_{\mathbf{t}}|\mathbf{t}\}) = \sum_{\mathbf{G}} c^{*}_{m,\mathbf{k}}(\mathcal{R}_{\mathbf{t}}\mathbf{k} - \mathbf{k} + \mathcal{R}_{\mathbf{t}}\mathbf{G}) c_{n,\mathbf{k}}(\mathbf{G}) \times e^{-i(\mathcal{R}_{\mathbf{t}}\mathbf{k}+\mathcal{R}_{\mathbf{t}}\mathbf{G})\cdot\mathbf{t}} \tag{18}$$

When spin-orbit coupling is taken into account, the Bloch wavefunctions become spinors. The transformation properties must then include the spin rotation induced by the symmetry operation. In this case, the representation generalizes to:

$$U^{m,n}_{\mathbf{k}}(\{\mathcal{R}_{\mathbf{t}}|\mathbf{t}\}) = \sum_{\sigma\sigma'} \mathcal{T}^{\sigma\sigma'}_{\mathcal{R}_{\mathbf{t}}} \langle m, \mathbf{k}, \sigma | \hat{P}_{\{\mathcal{R}_{\mathbf{t}}|\mathbf{t}\}} | n, \mathbf{k}, \sigma' \rangle \tag{19}$$

where $\mathcal{T}^{\sigma\sigma'}_{\mathcal{R}_{\mathbf{t}}}$ denotes the matrix elements of the spinor representation corresponding to the point group operation $\mathcal{R}_{\mathbf{t}}$. This formulation captures the combined effect of spatial and spin rotations on the symmetry behavior of Bloch spinors.

We have discussed the action of space group symmetries on Bloch wavefunctions, where spatial symmetry operations act through unitary transformations representing the real-space rotations, reflections, and translations, along with their corresponding action in reciprocal space. We now turn to the role of time-reversal symmetry, which differs fundamentally from space group operations due to its anti-unitary nature.

Time-reversal symmetry, unlike space group operations, reverses both the momentum and spin of a system and involves complex conjugation. In the spinless case, the time-reversal symmetry operator, $\hat{P}_{\Theta}$, reduces to the complex conjugation operator $\hat{\mathcal{C}}$, and relates Bloch states at $\mathbf{k}$ and $-\mathbf{k}$ through:

$$\hat{P}_{\Theta}\, |n, \mathbf{k}\rangle = |n, -\mathbf{k}\rangle \tag{20}$$

In position representation, using the identities $\hat{\mathcal{C}}^{\dagger}\mathbf{r}\hat{\mathcal{C}} = \mathbf{r}$ and $\hat{\mathcal{C}}^{\dagger}\mathbf{k}\hat{\mathcal{C}} = -\mathbf{k}$, this becomes:

$$\hat{P}_{\Theta}\psi_{n,\mathbf{k}}(\mathbf{r}) = \psi_{n,-\mathbf{k}}(\mathbf{r}) = \psi^{*}_{n,\mathbf{k}}(\mathbf{r}) \tag{21}$$

In the plane-wave basis, this implies the relation:

$$c_{n,-\mathbf{k}}(\mathbf{G}) = c^*_{n,\mathbf{k}}(-\mathbf{G}) \tag{22}$$

This relation allows wavefunctions at $-\mathbf{k}$ points in the BZ to be constructed from their time-reversal partners, $\mathbf{k}$, where they have been calculated explicitly. However, the $\mathbf{\Gamma}$ *i.e.* $\mathbf{k} = 0$, is a special point, as at this point $\mathbf{k} = -\mathbf{k}$. While the numerically obtained wavefunctions carry an arbitrary diagonalization phase, $e^{i\alpha_{n,\mathbf{k}}}$ at any $\mathbf{k}$ point for a band index n, this phase makes the Eq. 22 not to be automatically followed at the Γ point. In order to restore time-reversal symmetry at Γ, one can compute the following representation for each band:

$$\Theta_{n,\mathbf{\Gamma}} = \langle n, \mathbf{\Gamma}| \left(\hat{P}_\Theta \left| n, \mathbf{\Gamma} \right\rangle \right) = e^{-2i\alpha_{n,\mathbf{\Gamma}}} \tag{23}$$

The resulting quantity $\Theta_{n,\mathbf{\Gamma}}$ is a phase which can be used to construct time-reversal symmetric wavefunction as $|n, \mathbf{\Gamma}\rangle^{TR} = \sqrt{\Theta_{n,\mathbf{\Gamma}}}\, |n, \mathbf{\Gamma}\rangle$. Hereafter, the action of time-reversal symmetry will be denoted without explicitly writing the brackets on the right, with the understanding that it represents the operation itself.

For systems with spin-orbit coupling, time-reversal symmetry acts on spinor Bloch wavefunctions through the operator $\hat{P}^{sp}_\Theta = -i\sigma_y \hat{\mathcal{C}}$, where σ_y is the Pauli matrix acting in spin space. Its action in position representation on the spinor wavefunction is:

$$\begin{aligned} \hat{P}^{sp}_\Theta \Psi_{n,\mathbf{k}}(\mathbf{r}) &= \begin{bmatrix} \psi_{n,-\mathbf{k},\uparrow}(\mathbf{r}) \\ \psi_{n,-\mathbf{k},\downarrow}(\mathbf{r}) \end{bmatrix} = -i\sigma_y \hat{\mathcal{C}} \begin{bmatrix} \psi_{n,\mathbf{k},\uparrow}(\mathbf{r}) \\ \psi_{n,\mathbf{k},\downarrow}(\mathbf{r}) \end{bmatrix} \\ &= \begin{bmatrix} -\psi^*_{n,\mathbf{k},\downarrow}(\mathbf{r}) \\ \psi^*_{n,\mathbf{k},\uparrow}(\mathbf{r}) \end{bmatrix} \end{aligned} \tag{24}$$

In plane-wave basis, this leads to the following conditions:

$$c_{n,-\mathbf{k},\uparrow}(\mathbf{G}) = -c^*_{n,\mathbf{k},\downarrow}(-\mathbf{G}) \quad ; \quad c_{n,-\mathbf{k},\downarrow}(\mathbf{G}) = c^*_{n,\mathbf{k},\uparrow}(-\mathbf{G}) \tag{25}$$

To enforce this condition at the Γ point, one computes the time-reversal representation for spinor states analogous to spinless case, as described in Eq. 23. These symmetry constraints are essential for ensuring the correct transformation behavior of wavefunctions under time-reversal, particularly in systems with spin-orbit coupling and in the construction of time-reversal symmetric excitonic states, which will be discussed next.

B. Excitons and translational symmetry

The study of electron–hole excitations from the many-body ground state $|N, 0\rangle$ to an excited state $|N, S\rangle$ can be rigorously formulated within the framework of the two-particle Green's function and its equation of motion, the Bethe–Salpeter Equation (BSE) [34]. Here, S labels the excitation, while N denotes the conserved total number of electrons. Such excitations correspond to the creation of an electron in a conduction-band state and the removal of an electron from a valence-band state (equivalently, the creation of a hole).

Following the work of Strinati [34], the electron–hole amplitude is defined from the electron–hole correlation function as:

$$\Psi_S(\mathbf{x}, \mathbf{x}') = -\langle N, 0|\hat{\Psi}^\dagger(\mathbf{x}')\hat{\Psi}(\mathbf{x})|N, S\rangle \tag{26}$$

where $\hat{\Psi}^\dagger(\mathbf{x}')$ and $\hat{\Psi}(\mathbf{x})$ create and annihilate an electron at positions $\mathbf{x}'$ and $\mathbf{x}$, respectively.

Within the Tamm–Dancoff approximation (TDA), $\Psi_S(\mathbf{x}, \mathbf{x}')$ admits the expansion

$$\Psi_S(\mathbf{x}, \mathbf{x}') = \sum_v^{\text{occ}} \sum_c^{\text{empty}} A_{vc}^S \, \Psi_v^*(\mathbf{x}') \, \Psi_c(\mathbf{x}) \tag{27}$$

where $\Psi_v(\mathbf{x}')$ and $\Psi_c(\mathbf{x})$ are single-particle valence and conduction wave functions. The expansion coefficients are given by

$$A_{vc}^S \;=\; \langle N, 0 \,|\, \hat{b}_c \, \hat{a}_v \,|\, N, S\rangle \tag{28}$$

with $\hat{a}_v^\dagger$ creating a hole in state v and $\hat{b}_c^\dagger$ creating an electron in state c.

In periodic systems, the BSE Hamiltonian respects lattice translational symmetry. As a result, the two-particle translational operator $\hat{T}_{\mathbf{R}}^{\text{ex}}$ commutes with the BSE Hamiltonian $\hat{\mathcal{H}}_{\text{BSE}}$ (See Appendix A). This allows the excitations to be labeled by a conserved total momentum $\mathbf{Q}$, which is a good quantum number. The electron-hole amplitude associated with the finite momentum $\mathbf{Q}$ can then be written as:

$$\Psi_{S,\mathbf{Q}}(\mathbf{r}_e, \mathbf{r}_h) = \sum_{v,c,\mathbf{k}} A_{v,c,\mathbf{k}}^{S,\mathbf{Q}} \, \Psi_{c,\mathbf{k}}(\mathbf{r}_e) \, \Psi_{v,\mathbf{k}-\mathbf{Q}}^*(\mathbf{r}_h) \tag{29}$$

where $\Psi_{c,\mathbf{k}}(\mathbf{r}_e)$ and $\Psi_{v,\mathbf{k}-\mathbf{Q}}(\mathbf{r}_h)$ are Bloch wavefunctions evaluated at the electron and hole coordinates $\mathbf{r}_e$ and $\mathbf{r}_h$, respectively. From this point onward, we use the ket, $|\, S, \mathbf{Q}\rangle$, to represent the electron-hole amplitude state whose spatial representation is given in Eqn.

(29). Since the hole is generated by removing an electron at $\mathbf{k}-\mathbf{Q}$, its momentum is $-(\mathbf{k}-\mathbf{Q})=\mathbf{Q}-\mathbf{k}$. This allows it to be represented by the time-reversal of the valence-band electron state $|v,\mathbf{k}-\mathbf{Q}\rangle$. The excited state can thus be expressed in the product basis as:

$$|S,\mathbf{Q}\rangle=\sum_{v,c,\mathbf{k}} A^{S,\mathbf{Q}}_{v,c,\mathbf{k}}\,|v,\mathbf{k}-\mathbf{Q};\,c,\mathbf{k}\rangle \tag{30}$$

with

$$|v,\mathbf{k}-\mathbf{Q};\,c,\mathbf{k}\rangle=\hat{P}^h_\Theta\,|v,\mathbf{k}-\mathbf{Q}\rangle\otimes|c,\mathbf{k}\rangle \tag{31}$$

The excitonic Hilbert space is as a result a direct product of the electron and hole Hilbert spaces. Introducing center-of-mass and relative coordinates, $\mathbf{R}=\alpha\mathbf{r}_e+\beta\mathbf{r}_h$ (with $\alpha+\beta=1$) and $\mathbf{r}=\mathbf{r}_e-\mathbf{r}_h$ respectively, Eq. (29) takes the Bloch-periodic form

$$\Psi_{S,\mathbf{Q}}(\mathbf{R},\mathbf{r})=e^{i\mathbf{Q}\cdot\mathbf{R}}F_{S,\mathbf{Q}}(\mathbf{R},\mathbf{r}) \tag{32}$$

where the phase factor encodes the exciton's total momentum and $F_{S,\mathbf{Q}}(\mathbf{R},\mathbf{r})$ contains the cell-periodic structure (see Appendix A). This generalizes the single-particle Bloch theorem to the interacting two-particle excitonic case. The coefficients $A^{S,\mathbf{Q}}_{v,c,\mathbf{k}}$ and energies $\Omega_{S,\mathbf{Q}}$ are obtained by solving the BSE eigenvalue problem at fixed $\mathbf{Q}$:

$$\begin{aligned}&(\epsilon_{c,\mathbf{k}}-\epsilon_{v,\mathbf{k}-\mathbf{Q}})\,A^{S,\mathbf{Q}}_{v,c,\mathbf{k}}+\sum_{v',c',\mathbf{k}'}\langle v,\mathbf{k}-\mathbf{Q};c,\mathbf{k}|K^{eh}\\&|v',\mathbf{k}'-\mathbf{Q};c',\mathbf{k}'\rangle\,A^{S,\mathbf{Q}}_{v',c',\mathbf{k}'}=\Omega_{S,\mathbf{Q}}A^{S,\mathbf{Q}}_{v,c,\mathbf{k}}\end{aligned}$$

C. Excitons and Time-Reversal Symmetry

We begin by defining the time-reversal operator for excitons as the tensor product of the time-reversal operators acting individually on the valence hole and conduction electron:

$$\hat{P}^{ex}_\Theta=\hat{P}^h_\Theta\otimes\hat{P}^e_\Theta \tag{33}$$

Since the excitonic Hamiltonian commutes with the time-reversal operator, the exciton eigenstates at momentum $\mathbf{Q}$ and $-\mathbf{Q}$ are related by time-reversal symmetry (See Appendix B):

$$\Omega_{S,\mathbf{Q}}=\Omega_{S,-\mathbf{Q}},\quad \hat{P}^{ex}_\Theta\,|S,\mathbf{Q}\rangle=|S,-\mathbf{Q}\rangle \tag{34}$$

In the real-space representation, this relation resembles the transformation of single-particle wavefunctions under time-reversal and can be expressed as:

$$\hat{P}^{ex}_\Theta\Psi_{S,\mathbf{Q}}(\mathbf{r}_e,\mathbf{r}_h)=\Psi^*_{S,\mathbf{Q}}(\mathbf{r}_e,\mathbf{r}_h)=\Psi_{S,-\mathbf{Q}}(\mathbf{r}_e,\mathbf{r}_h) \tag{35}$$

We now derive the explicit transformation of the exciton expansion coefficients under time-reversal symmetry by examining the action of $\hat{P}^{ex}_{\Theta}$ on the excitonic state. The transformation takes the form:

$$
\begin{aligned}
|S, -\mathbf{Q}\rangle &= \hat{P}^{ex}_{\Theta}|S, \mathbf{Q}\rangle \\
&= \sum_{v,c,\mathbf{k}} (A^{S,\mathbf{Q}}_{v,c,\mathbf{k}})^* \left[\hat{P}^{h}_{\Theta}\hat{P}^{h}_{\Theta}|v, \mathbf{k}-\mathbf{Q}\rangle\right] \otimes \left[\hat{P}^{e}_{\Theta}|c, \mathbf{k}\rangle\right]
\end{aligned} \tag{36}
$$

As $\hat{P}^{ex}_{\Theta}$ is an anti-linear operator, it not only transforms the basis states but also complex conjugates the exciton coefficients.

Using the known time-reversal properties of the one-electron Bloch states, namely

$$
\hat{P}^{h}_{\Theta}|v, \mathbf{k}-\mathbf{Q}\rangle = |v, -\mathbf{k}+\mathbf{Q}\rangle, \quad \hat{P}^{e}_{\Theta}|c, \mathbf{k}\rangle = |c, -\mathbf{k}\rangle
$$

Eq. 36 becomes:

$$
\begin{aligned}
|S, -\mathbf{Q}\rangle &= \sum_{v,c,\mathbf{k}} (A^{S,\mathbf{Q}}_{v,c,\mathbf{k}})^* \left[\hat{P}^{h}_{\Theta}|v, -\mathbf{k}+\mathbf{Q}\rangle\right] \otimes |c, -\mathbf{k}\rangle \\
&= \sum_{v,c,\mathbf{k}} (A^{S,\mathbf{Q}}_{v,c,-\mathbf{k}})^* \left[\hat{P}^{h}_{\Theta}|v, \mathbf{k}+\mathbf{Q}\rangle\right] \otimes |c, \mathbf{k}\rangle
\end{aligned} \tag{37}
$$

By comparing this with the exciton state $|S, -\mathbf{Q}\rangle$ expressed in the product-state basis $\hat{P}^{h}_{\Theta}|v, \mathbf{k}+\mathbf{Q}\rangle \otimes |c, \mathbf{k}\rangle$, we identify the transformation law for the exciton wavefunction coefficients under time reversal:

$$
\tilde{A}^{S,-\mathbf{Q}}_{v,c,\mathbf{k}} = (A^{S,\mathbf{Q}}_{v,c,-\mathbf{k}})^* \tag{38}
$$

This result holds provided that the one-electron wavefunctions are constructed on a time-reversal symmetric $\mathbf{k}$-grid and are generated over the full Brillouin zone, ensuring time-reversal symmetry is preserved in both spinless and spinor systems. In particular, at $\mathbf{k} = 0$, the wavefunctions must explicitly satisfy time-reversal symmetry (See subsection A). This typically requires removing the arbitrary diagonalization phases at Γ, which can be achieved by computing the time-reversal representation matrices $\Theta_{n,\Gamma}$, as discussed in Eq. 23.

D. Excitons and space group symmetries

We define the action of a space group symmetry operation on the excitonic state as the tensor product of symmetry operators acting on the valence hole and conduction electron:

$$
\hat{P}^{ex}_{\{\mathcal{R}_{\mathbf{t}}|\mathbf{t}\}} = \hat{P}^{h}_{\{\mathcal{R}_{\mathbf{t}}|\mathbf{t}\}} \otimes \hat{P}^{e}_{\{\mathcal{R}_{\mathbf{t}}|\mathbf{t}\}} \tag{39}
$$

Since the Bethe-Salpeter Hamiltonian commutes with the excitonic symmetry operator, i.e., $[\hat{P}^{ex}_{\{\mathcal{R}_\mathbf{t}|\mathbf{t}\}}, \hat{\mathcal{H}}_{\text{BSE}}] = 0$, and the electron-hole amplitudes exhibit Bloch-periodicity under symmetry actions (See Appendix C), we obtain:

$$\Omega_{S,\mathcal{R}_\mathbf{t}\mathbf{Q}} = \Omega_{S,\mathbf{Q}}, \quad |S, \mathcal{R}_\mathbf{t}\mathbf{Q}\rangle = \hat{P}^{ex}_{\{\mathcal{R}_\mathbf{t}|\mathbf{t}\}}|S, \mathbf{Q}\rangle \tag{40}$$

This symmetry relation guarantees that excitonic eigenstates transform consistently under lattice symmetries, analogous to single-particle Bloch states.

Utilizing this framework, we can derive a relation between the coefficients $A^{S,\mathbf{Q}}_{v,c,\mathbf{k}}$ and those of the transformed state $\tilde{A}^{S,\mathcal{R}_\mathbf{t}\mathbf{Q}}_{v,c,\mathbf{k}}$, akin to the transformation properties of single-particle coefficients $c_{n,\mathbf{k}}(\mathbf{G})$ and $c^{\mathbf{t}}_{n,\mathcal{R}_\mathbf{t}\mathbf{k}}(\mathbf{G})$ as seen in Eq. 7.

The transformation of the excitonic state under symmetry becomes:

$$\begin{aligned} |S, \mathcal{R}_\mathbf{t}\mathbf{Q}\rangle &= \hat{P}^{ex}_{\{\mathcal{R}_\mathbf{t}|\mathbf{t}\}}|S, \mathbf{Q}\rangle = \\ &\sum_{v,c,\mathbf{k}} A^{S,\mathbf{Q}}_{v,c,\mathbf{k}} \left[\hat{P}^{h}_{\{\mathcal{R}_\mathbf{t}|\mathbf{t}\}}\hat{P}^{h}_{\Theta}|v, \mathbf{k}-\mathbf{Q}\rangle\right] \otimes \left[\hat{P}^{e}_{\{\mathcal{R}_\mathbf{t}|\mathbf{t}\}}|c, \mathbf{k}\rangle\right] \end{aligned} \tag{41}$$

and expanding the action of these operators in their respective degenerate subspaces, we obtain:

$$\begin{aligned} |S, \mathcal{R}_\mathbf{t}\mathbf{Q}\rangle = \sum_{v',c',\mathbf{k}} \Bigg[\sum_{v,c} & A^{S,\mathbf{Q}}_{v,c,\mathcal{R}_\mathbf{t}^{-1}\mathbf{k}} \mathcal{L}^{v',v}_{\mathbf{k}-\mathcal{R}_\mathbf{t}\mathbf{Q}}(\{\mathcal{R}_\mathbf{t}|\mathbf{t}\}) \\ & \otimes \mathcal{D}^{c',c}_{\mathbf{k}}(\{\mathcal{R}_\mathbf{t}|\mathbf{t}\})\Bigg] |v', \mathbf{k}-\mathcal{R}_\mathbf{t}\mathbf{Q}\rangle \otimes |c', \mathbf{k}\rangle \end{aligned} \tag{42}$$

where, the matrix elements for conduction and valence band transformations are defined as:

$$\mathcal{D}^{c',c}_{\mathbf{k}}(\{\mathcal{R}_\mathbf{t}|\mathbf{t}\}) = \langle c', \mathbf{k}|\hat{P}^{e}_{\{\mathcal{R}_\mathbf{t}|\mathbf{t}\}}|c, \mathcal{R}_\mathbf{t}{}^{-1}\mathbf{k}\rangle \tag{43}$$

$$\begin{aligned} \mathcal{L}^{v',v}_{\mathbf{k}-\mathcal{R}_\mathbf{t}\mathbf{Q}}(\{\mathcal{R}_\mathbf{t}|\mathbf{t}\}) &= \langle v', \mathbf{k}-\mathcal{R}_\mathbf{t}\mathbf{Q}|\, \hat{P}^{h}_{\Theta}\dagger \hat{P}^{h}_{\{\mathcal{R}_\mathbf{t}|\mathbf{t}\}} \\ \times\, \hat{P}^{h}_{\Theta}\,|v, \mathcal{R}_\mathbf{t}^{-1}\mathbf{k}-\mathcal{R}_\mathbf{t}\mathbf{Q})\rangle &= \left[\mathcal{D}^{v',v}_{\mathbf{k}-\mathcal{R}_\mathbf{t}\mathbf{Q}}(\{\mathcal{R}_\mathbf{t}|\mathbf{t}\})\right]^* \end{aligned} \tag{44}$$

The transformed exciton coefficients are then given by:

$$\begin{aligned} \tilde{A}^{S,\mathcal{R}_\mathbf{t}\mathbf{Q}}_{v,c,\mathbf{k}} = \sum_{v',c'} & A^{S,\mathbf{Q}}_{v',c',\mathcal{R}_\mathbf{t}{}^{-1}\mathbf{k}} \\ & \left[\mathcal{D}^{v,v'}_{\mathbf{k}-\mathcal{R}_\mathbf{t}\mathbf{Q}}(\{\mathcal{R}_\mathbf{t}|\mathbf{t}\})\right]^* \otimes \mathcal{D}^{c,c'}_{\mathbf{k}}(\{\mathcal{R}_\mathbf{t}|\mathbf{t}\}) \end{aligned} \tag{45}$$

This can be written compactly using matrix-vector multiplication, where the transformation matrix has elements:

$$\mathcal{M}^{\mathbf{k},\mathbf{Q}}_{v,c;v',c'}(\{\mathcal{R}_\mathbf{t}|\mathbf{t}\}) = [\mathcal{D}^{v,v'}_{\mathbf{k}-\mathcal{R}_\mathbf{t}\mathbf{Q}}(\{\mathcal{R}_\mathbf{t}|\mathbf{t}\})]^* \otimes \mathcal{D}^{c,c'}_{\mathbf{k}}(\{\mathcal{R}_\mathbf{t}|\mathbf{t}\}) \tag{46}$$

and the matrix form becomes:

$$\begin{aligned}
[\tilde{A}^{S,\mathcal{R}_\mathbf{t}\mathbf{Q}}_{\mathbf{k}}]_{v,c} &= \sum_{v',c'} \mathcal{M}^{\mathbf{k},\mathbf{Q}}_{v,c;v',c'}(\{\mathcal{R}_\mathbf{t}|\mathbf{t}\}) A^{S,\mathbf{Q}}_{v',c',\mathcal{R}_\mathbf{t}^{-1}\mathbf{k}} \\
&= \left[\mathcal{M}^{\mathbf{k},\mathbf{Q}}(\{\mathcal{R}_\mathbf{t}|\mathbf{t}\}) \cdot A^{S,\mathbf{Q}}_{\mathcal{R}_\mathbf{t}^{-1}\mathbf{k}}\right]_{v,c}
\end{aligned} \tag{47}$$

Thus, the transformation of the exciton coefficient vector at each **k**-point simplifies to:

$$\tilde{A}^{S,\mathcal{R}_\mathbf{t}\mathbf{Q}}_{\mathbf{k}} = \mathcal{M}^{\mathbf{k},\mathbf{Q}}(\{\mathcal{R}_\mathbf{t}|\mathbf{t}\}) \cdot A^{S,\mathbf{Q}}_{\mathcal{R}_\mathbf{t}^{-1}\mathbf{k}} \tag{48}$$

When dealing with spinor wavefunctions, the symmetry operator $\hat{P}^{h/e}_{\{\mathcal{R}_\mathbf{t}|\mathbf{t}\}}$ must be replaced with the product $\hat{P}^{h/e}_{\{\mathcal{R}_\mathbf{t}|\mathbf{t}\}} \otimes \hat{\mathcal{T}}^{v/c}_{\mathcal{R}_\mathbf{t}}$, where $\hat{\mathcal{T}}_{\mathcal{R}_\mathbf{t}}$ denotes the SU(2) rotation corresponding to the SO(3) spatial symmetry $\mathcal{R}_\mathbf{t}$. This ensures that spinor structure is correctly accounted for, consistent with the representation theory described in Eq. 14.

E. Symmetry classification of excitons

Exciton bands can be classified according to the irreducible representations of the symmetry group, in analogy with single-particle bands. This classification is possible now that we have established how excitonic states transform under symmetry operations. The definition of the little group is also analogous, with the key distinction being that for excitons, it is defined with respect to the center-of-mass (COM) momentum $\mathbf{Q}$. The little group $\mathcal{G}_\mathbf{Q}$ consists of all symmetry operations $\{\mathcal{R}_\mathbf{t}|\mathbf{t}\}$ that leave $\mathbf{Q}$ invariant up to a reciprocal lattice vector, i.e., $\mathcal{R}_\mathbf{t}\mathbf{Q} = \mathbf{Q} \pm \mathbf{G}$. For any such $\{\mathcal{R}_\mathbf{t}|\mathbf{t}\} \in \mathcal{G}_\mathbf{Q}$, the excitonic state $|S, \mathbf{Q}\rangle$ transforms as:

$$\hat{P}^{ex}_{\{\mathcal{R}_\mathbf{t}|\mathbf{t}\}}|S, \mathbf{Q}\rangle = \sum_{S'=1}^{N_{exc}} \mathcal{K}^{S',S}_{\mathbf{Q}}(\{\mathcal{R}_\mathbf{t}|\mathbf{t}\})|S', \mathbf{Q}\rangle \tag{49}$$

Here, $\mathcal{K}_\mathbf{Q}(\{\mathcal{R}_\mathbf{t}|\mathbf{t}\})$ forms a representation of the little group $\mathcal{G}_\mathbf{Q}$ within the invariant subspace spanned by the excitonic states $\{|S, \mathbf{Q}\rangle\}_{N_{exc}}$. Its matrix elements are given by:

$$\mathcal{K}^{S',S}_{\mathbf{Q}}(\{\mathcal{R}_\mathbf{t}|\mathbf{t}\}) = \langle S', \mathbf{Q}|\hat{P}^{ex}_{\{\mathcal{R}_\mathbf{t}|\mathbf{t}\}}|S, \mathbf{Q}\rangle \tag{50}$$

The action of $\hat{P}^{ex}_{\{\mathcal{R}_\mathbf{t}|\mathbf{t}\}}$ on $|S, \mathbf{Q}\rangle$, using Eqs. 41 and 48, leads to:

$$\hat{P}^{ex}_{\{\mathcal{R}_\mathbf{t}|\mathbf{t}\}}|S, \mathbf{Q}\rangle = \sum_{v',c',\mathbf{k}'} A^{S,\mathbf{Q}}_{v',c',\mathbf{k}'}[\hat{P}^h_\Theta|v', \mathbf{k}' - \mathbf{Q}\rangle] \otimes |c', \mathbf{k}'\rangle \tag{51}$$

To compute the matrix elements of the representation, we expand $|S', \mathbf{Q}\rangle$ in the electron-hole basis and evaluate the overlap:

$$\begin{aligned}\mathcal{K}^{S',S}_\mathbf{Q}(\{\mathcal{R}_\mathbf{t}|\mathbf{t}\}) = &\sum_{v,c,v',c',\mathbf{k},\mathbf{k}'} (A^{S',\mathbf{Q}}_{v,c,\mathbf{k}})^* \tilde{A}^{S,\mathbf{Q}}_{v',c',\mathbf{k}'} \\ &\langle v, \mathbf{k} - \mathbf{Q}|\hat{P}^{h\dagger}_\Theta \hat{P}^h_\Theta|v', \mathbf{k}' - \mathbf{Q}\rangle\langle c, \mathbf{k}|c', \mathbf{k}'\rangle\end{aligned} \tag{52}$$

Using orthonormality of the electronic states and $\hat{P}^{h,\dagger}_\Theta \hat{P}^h_\Theta = I$, this expression simplifies to:

$$\mathcal{K}^{S',S}_\mathbf{Q}(\{\mathcal{R}_\mathbf{t}|\mathbf{t}\}) = \sum_{v,c,v',c',\mathbf{k},\mathbf{k}'} (A^{S',\mathbf{Q}}_{v,c,\mathbf{k}})^* \tilde{A}^{S,\mathbf{Q}}_{v',c',\mathbf{k}'} \delta_{v,v'}\delta_{c,c'}\delta_{\mathbf{k},\mathbf{k}'} \tag{53}$$

yielding:

$$\mathcal{K}^{S',S}_\mathbf{Q}(\{\mathcal{R}_\mathbf{t}|\mathbf{t}\}) = \sum_{v,c,\mathbf{k}} (A^{S',\mathbf{Q}}_{v,c,\mathbf{k}})^* \tilde{A}^{S,\mathbf{Q}}_{v,c,\mathbf{k}} \tag{54}$$

Finally, using Eq. 48, we obtain a compact form:

$$\mathcal{K}^{S',S}_\mathbf{Q}(\{\mathcal{R}_\mathbf{t}|\mathbf{t}\}) = \sum_{v,c,\mathbf{k}} \left[A^{S',\mathbf{Q}}_\mathbf{k}\right]^*_{v,c} \left[\mathcal{M}^{\mathbf{k},\mathbf{Q}}(\{\mathcal{R}_\mathbf{t}|\mathbf{t}\}) A^{S,\mathbf{Q}}_{\mathcal{R}_\mathbf{t}^{-1}\mathbf{k}}\right]_{v,c} \tag{55}$$

Each representation $\mathcal{K}_\mathbf{Q}$ is characterized by its trace, known as the character:

$$\mathcal{X}_{\mathcal{K}_\mathbf{Q}}(\{\mathcal{R}_\mathbf{t}|\mathbf{t}\}) = \mathrm{Tr}\big[\mathcal{K}_\mathbf{Q}(\{\mathcal{R}_\mathbf{t}|\mathbf{t}\})\big] = \sum_S \mathcal{K}^{S,S}_\mathbf{Q}(\{\mathcal{R}_\mathbf{t}|\mathbf{t}\}) \tag{56}$$

In general, the invariant subspace spanned by $\{|S, \mathbf{Q}\rangle\}_{N_{exc}}$ may decompose into a direct sum of multiple irreducible representations. Therefore, the representation $\mathcal{K}_\mathbf{Q}$ may be reducible and can be expressed as:

$$\mathcal{K}_\mathbf{Q} = \oplus_\xi m^\xi_\mathbf{Q} \mathcal{K}^\xi_\mathbf{Q} \tag{57}$$

Here, $\mathcal{K}^\xi_\mathbf{Q}$ is the ξ^{th} irreducible representation of $\mathcal{G}_\mathbf{Q}$, and $m^\xi_\mathbf{Q}$ denotes its multiplicity within $\mathcal{K}_\mathbf{Q}$. This multiplicity can be computed using:

$$m^\xi_\mathbf{Q} = \frac{1}{N_{\mathcal{G}_\mathbf{Q}}} \sum_{\{\mathcal{R}_\mathbf{t}|\mathbf{t}\}\in\mathcal{G}_\mathbf{Q}} \mathcal{X}^*_{\mathcal{K}_\mathbf{Q}}(\{\mathcal{R}_\mathbf{t}|\mathbf{t}\})\mathcal{X}_\xi(\{\mathcal{R}_\mathbf{t}|\mathbf{t}\}) \tag{58}$$

where $N_{\mathcal{G}_\mathbf{Q}}$ is the order of the group, and $\mathcal{X}_\xi(\{\mathcal{R}_\mathbf{t}|\mathbf{t}\})$ is the character of the ξ^{th} irreducible representation, which can be obtained from symmetry tools such as SPGREP.

To assign each excitonic state to a specific irreducible representation, we use the corresponding projection operator:

$$\hat{\mathcal{V}}^{(\xi)}_{ij;\mathbf{Q}} = \frac{d_\xi}{N_{\mathcal{G}_\mathbf{Q}}} \sum_{\{\mathcal{R}_\mathbf{t}|\mathbf{t}\}\in\mathcal{G}_\mathbf{Q}} \left[\Delta^{(\xi)}_{ij}(\{\mathcal{R}_\mathbf{t}|\mathbf{t}\})\right]^* \hat{P}^{ex}_{\{\mathcal{R}_\mathbf{t}|\mathbf{t}\}} \tag{59}$$

Here, $\hat{\mathcal{V}}^{(\xi)}_{ij;\mathbf{Q}}$ projects onto the subspace transforming as the irreducible representation ξ, d_ξ is its dimension, and $\Delta^{(\xi)}_{ij}$ is the matrix representation of the symmetry operation.

Symmetry-based classification of excitons provides significant physical insight. States transforming under one-dimensional irreducible representations are non-degenerate, whereas higher-dimensional irreducible representations give rise to degeneracies. These degeneracies can be lifted by perturbations such as spin-orbit coupling or external fields. Moreover, the symmetry of excitonic states plays a crucial role in determining optical selection rules and polarization properties.

F. Symmetry-adapted reduction in the BSE Hamiltonian

For space group operations $\{\mathcal{R}_\mathbf{t}|\mathbf{t}\} \in \mathcal{G}$, the excitonic symmetry operator commutes with the Bethe-Salpeter Hamiltonian, i.e., $[\hat{P}^{ex}_{\{\mathcal{R}_\mathbf{t}|\mathbf{t}\}}, \hat{\mathcal{H}}_{\text{BSE}}] = 0$. This invariance under symmetry operations implies that the Hamiltonian blocks at exciton center-of-mass momenta $\mathbf{Q}$ and $\mathcal{R}_\mathbf{t}\mathbf{Q}$ are related as:

$$\hat{P}_{\{\mathcal{R}_\mathbf{t}|\mathbf{t}\}}\, \hat{\mathcal{H}}^{\text{BSE}}_\mathbf{Q}\, \hat{P}^{-1}_{\{\mathcal{R}_\mathbf{t}|\mathbf{t}\}} = \hat{\mathcal{H}}^{\text{BSE}}_{\mathcal{R}_\mathbf{t}\mathbf{Q}} \tag{60}$$

This means that for operations not in the little group $\mathcal{G}_\mathbf{Q}$, the symmetry connects different momentum sectors. However, when $\{\mathcal{R}_\mathbf{t}|\mathbf{t}\} \in \mathcal{G}_\mathbf{Q}$, i.e., they leave $\mathbf{Q}$ invariant, the Hamiltonian satisfies:

$$\hat{P}_{\{\mathcal{R}_\mathbf{t}|\mathbf{t}\}}\, \hat{\mathcal{H}}^{\text{BSE}}_\mathbf{Q}\, \hat{P}^{-1}_{\{\mathcal{R}_\mathbf{t}|\mathbf{t}\}} = \hat{\mathcal{H}}^{\text{BSE}}_{\mathbf{Q}} \tag{61}$$

Thus, $\hat{\mathcal{H}}^{\text{BSE}}_\mathbf{Q}$ transforms as a representation of the little group $\mathcal{G}_\mathbf{Q}$. In cases where this representation is reducible, as commonly happens at high-symmetry points like $\mathbf{Q} = 0$ or others with less symmetries, the Hamiltonian can be block-diagonalized into subspaces associated with irreducible representations, greatly simplifying the diagonalization.

We now outline the general formalism for constructing symmetry-adapted irreducible blocks of the Hamiltonian, valid at both zero and finite $\mathbf{Q}$. A key step involves using the projection operators (defined in Eq. 59), which were earlier used for exciton classification.

Here, they serve to build symmetry-adapted product state bases that isolate irreducible subspaces of the Hilbert space, enabling block-diagonalization.

By applying these projectors to the exciton product basis defined in Eq. 31, and using the transformation law in Eq. 15, we obtain the symmetry-adapted basis:

$$\begin{aligned}
&\tilde{\phi}^{(\xi)}_{(i,j);v,c,\mathbf{k},\mathbf{Q}} = \hat{\mathcal{V}}^{(\xi)}_{ij;\mathbf{Q}}|v,\mathbf{k}-\mathbf{Q};\, c,\mathbf{k}\rangle \\
&= \frac{d_\xi}{N_{\mathcal{G}_\mathbf{Q}}} \sum_{\{\mathcal{R}_\mathbf{t}|\mathbf{t}\}\in\mathcal{G}_\mathbf{Q}} \left[\Delta^{(\xi)}_{ij}(\{\mathcal{R}_\mathbf{t}|\mathbf{t}\})\right]^* \hat{P}^{ex}_{\{\mathcal{R}_\mathbf{t}|\mathbf{t}\}}|v,\mathbf{k}-\mathbf{Q};\, c,\mathbf{k}\rangle \\
&= \frac{d_\xi}{N_{\mathcal{G}_\mathbf{Q}}} \sum_{v',c',\{\mathcal{R}_\mathbf{t}|\mathbf{t}\}\in\mathcal{G}_\mathbf{Q}} \left[\Delta^{(\xi)}_{ij}(\{\mathcal{R}_\mathbf{t}|\mathbf{t}\})\right]^* \left[\mathcal{D}^{v',v}_{\mathcal{R}_\mathbf{t}\mathbf{k}-\mathbf{Q}}(\{\mathcal{R}_\mathbf{t}|\mathbf{t}\})\right]^* \\
&\otimes \mathcal{D}^{c',c}_{\mathcal{R}_\mathbf{t}\mathbf{k}}(\{\mathcal{R}_\mathbf{t}|\mathbf{t}\})|v',\mathcal{R}_\mathbf{t}\mathbf{k}-\mathbf{Q};\, c',\mathcal{R}_\mathbf{t}\mathbf{k}\rangle
\end{aligned} \tag{62}$$

Here, $\mathbf{k} \in$ IBZ, and the set $\{\tilde{\phi}^{(\xi)}_{(i,j);v,c,\mathbf{k},\mathbf{Q}}\}$ forms a symmetry-adapted basis for the irreducible representation ξ, with $i, j = 1, \ldots, d_\xi$.

When the BSE Hamiltonian is expressed in this basis, it takes a block-diagonal form:

$$\begin{bmatrix}
\mathcal{H}^{(\xi_1)} & 0 & 0 & \cdots & 0 \\
0 & \mathcal{H}^{(\xi_2)} & 0 & \cdots & 0 \\
0 & 0 & \mathcal{H}^{(\xi_3)} & \cdots & 0 \\
\vdots & \vdots & \vdots & \ddots & \vdots \\
0 & 0 & 0 & \cdots & \mathcal{H}^{(\xi_n)}
\end{bmatrix} \tag{63}$$

Each block $\mathcal{H}^{(\xi_i)}$ represents an independent sector corresponding to the irreducible representation ξ_i of $\mathcal{G}_\mathbf{Q}$.

This decomposition stems directly from group representation theory, where the exciton basis and symmetry operators form a reducible representation. Projection operators allow one to isolate irreducible sectors, ensuring orthogonality and eliminating coupling between different symmetry blocks.

Physically, these blocks correspond to excitonic states categorized by their symmetry. This classification is useful for identifying bright and dark excitons depending on their symmetry behavior under optical transitions. Computationally, this structure enables solving several smaller eigenvalue problems rather than a single large one, making the BSE calculations more tractable and symmetry-respecting.

III. COMPUTATIONAL DETAILS

For our calculations, we used the experimental in-plane lattice constants for monolayer MoS_2 (3.168 Å, S-S distance of 3.133 Å). A vacuum spacing of 16 Å was introduced along the out-of-plane direction to avoid spurious interactions between periodic images.

Density functional theory (DFT) calculations were performed with the Quantum Espresso [18, 35] package using the PBE generalized gradient approximation(GGA) [36] for the exchange-correlation functional. The wavefunctions were expanded in plane waves up to an energy cutoff of 90 Ry. Spin-orbit coupling was explicitly included by using fully relativistic optimized norm-conserving Vanderbilt pseudopotentials [37] from the PseudoDojo [38] library. Self-consistent calculations were performed on a $24 \times 24 \times 1$ $\mathbf{k}$-grid, resulting in DFT band gap of 1661.9 meV for MoS_2.

Quasiparticle energies were obtained within the G_0W_0 [39] approximation using the BerkeleyGW package [9, 11, 40], starting from the DFT wavefunctions and eigenvalues computed with Quantum Espresso. We employed the spinor implementation of BerkeleyGW [41], wherein spin-orbit coupling is included non-perturbatively. The dielectric function was evaluated using the generalized plasmon-pole model of Hybertsen and Louie [39], with a $6\times6\times1$ $\mathbf{q}$-grid and 4000 occupied and unoccupied bands. Plane waves up to an energy cutoff of 25 Ry were used in the computation of dielectric function. The Brillouin-zone sampling was refined near $\mathbf{q} = 0$ using a non-uniform neck subsampling(NNS) [42] scheme with a fine non-uniform sampling of 10 points. Coulomb truncation was applied along the out-of-plane direction to eliminate interlayer interactions [43]. The resulting GW gap at the K point was 2553.9 meV for MoS_2.

The Bethe-Salpeter equation (BSE) was solved within the Tamm-Dancoff approximation using BerkeleyGW [9, 11, 40, 41]. BSE calculations were performed for finite-$\mathbf{Q}$ points along the path Γ-M-K-Γ of the Brillouin Zone. The electron-hole interaction kernel and absorption calculations were done on a $24 \times 24 \times 1$ $\mathbf{k}$-grid with 2 valence and 4 conduction bands. The dielectric matrix was evaluated using plane waves up to the energy cutoff of 5 Ry in the BSE kernel calculations. One-electron wavefunctions at all the $\mathbf{k}$-points in the full Brillouin zone were constructed by rotating the wavefunctions generated in the irreducible Brillouin zone to preserve phase consistency at symmetry-related points.

IV. RESULTS AND DISCUSSION

The formalism that we have developed in section II is general. We use monolayer MoS_2 as a prototypical example to show the application of this formalism within an *ab initio* context. The nomenclature and labels used to represent the groups and their irreducible representations are adopted from Ref. [44]. The crystal symmetry of monolayer MoS_2 is described by the point group D_{3h}. The little group at the center of the Brillouin zone ($\mathbf{k} = \Gamma$), $\mathcal{G}_\Gamma$, contains all the symmetry elements of the D_{3h} group. At other high-symmetry points in the Brillouin zone the little groups contain fewer symmetry elements—for example, at $\mathbf{k} = \mathrm{M}$ the little group, $\mathcal{G}_\mathrm{M}$, is C_{2v}, while at $\mathbf{k} = \mathrm{K}$, the little group, $\mathcal{G}_\mathrm{K}$, is C_{3h}. In the absence of spin-orbit coupling, the one-electron eigenstates are also eigenstates of the spin angular momentum operator. As a result, they can be labeled using the single-group irreducible representations of the little groups listed above. As our calculations include spin–orbit coupling, the one-electron eigenstates are spinors as they are not eigenstates of the spin angular momentum operator. Consequently, the associated irreducible representations belong to the complex double groups, D_{3h}^D, C_{2v}^D, and C_{3h}^D at the Γ, M, and K points in the Brillouin zone, respectively.

Fig. 1(a) shows the quasiparticle band structure obtained using the $\mathrm{G_0W_0}$ approximation to the self energy. The bands are plotted along the high-symmetry path $\Gamma - \mathrm{M} - \mathrm{K} - \Gamma$. We use the diagonal approximation of $\mathrm{G_0W_0}$ to calculate the quasiparticle energies. Within this approximation, the quasiparticle wavefunctions are assumed to be the same as the corresponding DFT wavefunctions and the self-energy operator only corrects the DFT eigenvalues to the corresponding quasiparticle energy. As a result, we use the DFT spinor wavefunctions to calculate the irreducible representations of the corresponding complex double groups at the high-symmetry points. Fig. 1(a) also shows the assignments of the irreducible representations at the high-symmetry points to the states that are closest to the band gap. For the first two valence and four conduction states at the Γ point, the doubly degenerate states can be labeled by the irreducible representations Γ_7, Γ_7, and Γ_9 respectively. At the M point in the Brillouin zone, the labels are M_5 for each pair of doubly degenerate states. At the K point, the one-dimensional representations of the valence bands are K_{12} and K_{10}, respectively, and the representations are K_7, K_8, K_{11}, and K_8 for the spin–orbit split, non-degenerate states in the conduction band manifold. These irreducible representations are the same as those calculated from the IrRep package [7].

In contrast to quasiparticles, excitons are composite bosons. The excitonic states are written as a linear combination of basis states constructed from the tensor product of two fermionic states—electron and hole. In the absence of spin-orbit coupling, the total spin angular momentum of these basis states is given by the addition of the spin angular momenta of the constituent electron and hole states. This leads to the excitonic states being eigenstates of the total spin angular momentum operator. They are characterized by the eigenvalues of the square of the total spin operator, S^2, ($2\hbar^2$ for triplets and $\hbar^2$ for singlets) and S_z, the spin projection operator along the z-axis ($-1, 0, 1$ for triplets and 0 for singlets). In the presence of spin-orbit coupling, when the one-electron states are no longer eigenstates of the spin angular momentum operator, the resulting excitons are also no longer eigenstates of the total spin angular momentum operator. Then, the excitonic eigenstates are linear combinations of singlet and triplet states. Nevertheless, in both cases (in the presence or absence of spin orbit coupling), the symmetry classification of excitonic states is governed by the single-group irreducible representations of the little group at the center-of-mass momentum $\mathbf{Q}$ of the exciton. Thus, the relevant irreducible representations of the excitonic states are those of the single groups D_{3h}, C_{2v} and C_{3h} for $\mathbf{Q} = \Gamma$, $\mathbf{Q} = \mathrm{M}$ and $\mathbf{Q} = \mathrm{K}$, respectively.

We implemented the formalism for applying spatial and time-reversal symmetries to excitonic states, as described in Sections II C and II D. In order to test the implementation, as a first step, we calculated the excitonic states at a point $\mathbf{Q}$ in the irreducible Brillouin zone. Upon rotating these states by a space group symmetry operation, $\{\mathcal{R}_\mathbf{t}|\mathbf{t}\}$, we obtained the excitonic states at the point $\mathcal{R}_\mathbf{t}\mathbf{Q}$. We compared these states to the corresponding excitonic states directly calculated at the rotated momentum $\mathcal{R}_\mathbf{t}\mathbf{Q}$. In an analogous manner, we compared the time-reversed exciton states at $\mathbf{Q}$ and $-\mathbf{Q}$. In both cases, we found exact agreement, up to an overall diagonalization phase, thereby confirming the correctness of our implementation of both space-group and time-reversal symmetries.

Our implementation also allows for the direct computation of irreducible representations of the invariant subspaces within the exciton manifold at a given $\mathbf{Q}$ and their characters from the excitonic states, using Eqs. 55 and 58 (Subsection II F). Using this approach, we obtained the irreducible representations of excitonic bands along the high-symmetry path $\Gamma - \mathrm{M} - \mathrm{K} - \Gamma$ in the Brillouin zone, as shown in Fig. 1(b). Consider the case $\mathbf{Q} = 0$: the 1s-like A excitons (A_{1s}) originate from the top valence band (VB_1) and the two lowest conduction bands (CB_1 and CB_2), near the K/$-$K valleys [45]. The complex double-group irreducible representations for VB_1, CB_1, and CB_2 are K_{10}, K_7, and K_8 at the K valley (see Fig. 1), with conjugate irreducible representations K_9, K_8, and K_7 at the $-$K valley. The transitions between CB_1 and VB_1 at the K and $-$K valley, yield direct product states with irreducible representations given as: $K_7^* \otimes K_{10} = K_3$ and $K_8^* \otimes K_9 = K_2$, respectively. If the exciton envelope function of $1s$ excitonic states transforms as K_1, the resulting $1s$-like excitonic states correspond to $K_3 \oplus K_2$. For the transitions involving CB_2 and VB_1 at the K and $-$K valley, we obtain the direct product states with irreducible representations as $K_8^* \otimes K_{10} = K_4$ and $K_7^* \otimes K_9 = K_4$, respectively. As these transitions form the basis for excitons at $\mathbf{Q} = \Gamma$ point in the excitonic band structure, we use the compatibility relation for $C_{3h} \to D_{3h}$. This compatibility relation maps these irreducible representations at K to irreducible representations at $\mathbf{Q} = \Gamma$ as: $K_3 \oplus K_2 \to \Gamma_6$ and $K_4/K_4 \to \Gamma_3/\Gamma_4$. Hence, the first four A_{1s} excitons transform as $\Gamma_3 \oplus \Gamma_4 \oplus \Gamma_6$. The classification obtained from our implementation is fully consistent with the physical and conceptual classification for A_{1s} excitons (See Fig. 1b and Table. I).

We next analyze the $1s$-like B excitons (B_{1s}), which originate from the valence band (VB_2) and the two lowest conduction bands (CB_1 and CB_2). The complex double-group irreducible representations for VB_2 at the K and $-$K valley is K_{10} and K_{11}, respectively. The irreducible representations of the direct product of states corresponding to the transitions between CB_1 and VB_2 at K and $-$K valley are $K_7^* \otimes K_{12} = K_5$ and $K_8^* \otimes K_{11} = K_6$, respectively. If the exciton envelope function of $1s$ transforms as K_1, the corresponding direct product states are $K_5 \oplus K_6$. For the transitions involving CB_2 and VB_2 at K and $-$K valley, we obtain $K_8^* \otimes K_{12} = K_3$ and $K_7^* \otimes K_{11} = K_2$, respectively, leading to the states belonging to $K_3 \oplus K_2$. As discussed before, using the compatibility relation for $C_{3h} \to D_{3h}$, this maps as $K_5 \oplus K_6 \to \Gamma_5$ and $K_3 \oplus K_2 \to \Gamma_6$. Therefore, the next four B_{1s} excitons at the $\mathbf{Q} = \Gamma$ transform as $\Gamma_5 \oplus \Gamma_6$. The classification obtained from our symmetry formalism is fully consistent with the physical and conceptual classification for B_{1s} excitons, as well. (See Fig. 1b and Table. I).

Furthermore, we verified the validity of the irreducible representations at various finite center-of-mass momenta of excitons by explicitly tracking the compatibility relations between transitions of different symmetry groups at the high-symmetry points and the connecting symmetry lines. For Σ_{pt_1} on the symmetry line Σ, the symmetry elements that form the group are $\{E, C_2, \sigma_h, \sigma_v\}$, which is isomorphic to the C_{2v} group with symmetry elements $\{E, C_2, \sigma_v, \sigma_v'\}$ and the same character table. This group has four one-dimensional irreducible representations, denoted $\Sigma_1, \Sigma_2, \Sigma_3, \Sigma_4$. The compatibility relations from $D_{3h} \to C_{2v}$ are given by

$$\Gamma_3 \to \Sigma_3, \quad \Gamma_4 \to \Sigma_4, \quad \Gamma_6 \to \Sigma_1 \oplus \Sigma_2, \quad \Gamma_5 \to \Sigma_3 \oplus \Sigma_4,$$

which is in exact agreement with the independent symmetry classification obtained from our implementation. Higher-lying states are expected to follow the order predicted by these compatibility relations. However, due to band crossings and the presence of nearly degenerate states, the ordering of irreducible representations can change. This highlights the advantage of an explicit symmetry classification of excitonic bands, as it allows one to consistently identify states belonging to the same irreducible representations and to track them reliably, especially in the case of fine **k**-point sampling where significant exciton overlap occurs between nearby points.

As one traverses the Σ line toward Σ_{pt_2}, the ordering of the symmetry irreducible representations of the states changes. The irreducible representations obtained at Σ_{pt_2} remain compatible with those at the M point, since the symmetry group is the same along the Σ direction and $\mathbf{Q} = \mathrm{M}$. We then consider the T high-symmetry line from M to K. Along this path, from the M point to T_{pt_1}, the group reduces as $C_{2v} \to C_s = \{E, \sigma_h\}$. This group has two one-dimensional irreducible representations, with characters 1 and -1 under σ_h, labeled as T_1 and T_2. Since the characters of σ_h for M_3 and M_4 are -1, while those for M_1 and M_2 are 1, the compatibility relations are

$$\mathrm{M}_3/\mathrm{M}_4 \to \mathrm{T}_2, \quad \mathrm{M}_1/\mathrm{M}_2 \to \mathrm{T}_1.$$

This relation holds for the first seven exciton states (see Table I), although the eighth and ninth states are accidentally degenerate in energy (i.e., not symmetry-protected). Consequently, the eighth exciton state at M is compatible with the ninth state at T_{pt_1}.

Following these connectivities, the irreducible representations at T_{pt_2} are shown in Fig. I. One observes that some states shift within the manifold to preserve compatibility relations at the transition from T_{pt_2} to K, where the symmetry changes from $C_{2v} \to C_{3h}$. The little group at $\mathbf{Q} = \mathrm{K}$ is C_{3h}, consisting of the symmetry elements $\{E, C_3, C_3^{-1}, \sigma_h, S_3, S_3^{-1}\}$. This group has six one-dimensional irreducible representations, labeled K_1 through K_6. The characters of σ_h are -1 for $\mathrm{K}_4, \mathrm{K}_5, \mathrm{K}_6$, and $+1$ for $\mathrm{K}_1, \mathrm{K}_2, \mathrm{K}_3$. Thus, the compatibility relations between

T_{pt_2} and K are

$$\mathrm{K}_4, \mathrm{K}_5, \mathrm{K}_6 \rightarrow \mathrm{T}_2, \quad \mathrm{K}_1, \mathrm{K}_2, \mathrm{K}_3 \rightarrow \mathrm{T}_1.$$

This correspondence is observed in our computed classifications, with the exception of the eighth state at K, which was found to be compatible with the ninth state at T_{pt_2}, again because of similar reasons discussed before.

Along the Λ line, one can similarly follow the compatibility relations from $C_{3h} \rightarrow C_s$. From Λ_{pt_2} to Γ *i.e.* from $C_s \rightarrow D_{3h}$, the characters of σ_h are $-1, -1, 2$ for $\Gamma_3, \Gamma_4, \Gamma_6$, respectively, and $1, 1, -2$ for $\Gamma_1, \Gamma_2, \Gamma_5$, respectively. Therefore, the compatibility relations are

$$\Gamma_3, \Gamma_4 \rightarrow \Lambda_2, \quad \Gamma_1, \Gamma_2 \rightarrow \Lambda_1, \quad \Gamma_5 \rightarrow \Lambda_2 \oplus \Lambda_2, \quad \Gamma_6 \rightarrow \Lambda_1 \oplus \Lambda_1.$$

Our results are in excellent agreement with these predicted compatibility relations.

In addition to proposing and implementing a formalism for symmetry-based classification of excitonic states, we employed projection operators (see subsection II F) to construct the symmetry-adapted linear combinations of the electron-hole direct-product-state basis for every irreducible representation of the little group $\mathcal{G}_{\mathbf{Q}}$. This procedure not only block-diagonalizes the BSE Hamiltonian at that $\mathbf{Q}$ point into smaller blocks corresponding to distinct irreducible representations, but also provides an independent route for characterizing the excitons. We demonstrated this reduction explicitly for $\mathbf{Q} = \Gamma$ and $\mathbf{Q} = \mathrm{K}$ in Fig. 2. The exciton states obtained from diagonalization within each irreducible representation block coincides with those obtained through direct symmetry classification, confirming consistency between the two methods. The agreement of exciton irreducible representations with both the physical interpretation of compatibility relations and the block-diagonalization procedure establishes the robustness of our formalism.

V. CONCLUSIONS

In summary, in this paper we have established a general symmetry-based framework for excitons, incorporating both time-reversal and space-group operations. We showed how one can generate the excitonic states within the irreducible Brillouin zone and use space group symmetry operations to obtain the states at other points in the full Brillouin zone. This method allows great reduction in computational cost especially in problems where a fine sampling of the excitonic centre-of-mass moementum is needed. Furthermore, by explicitly

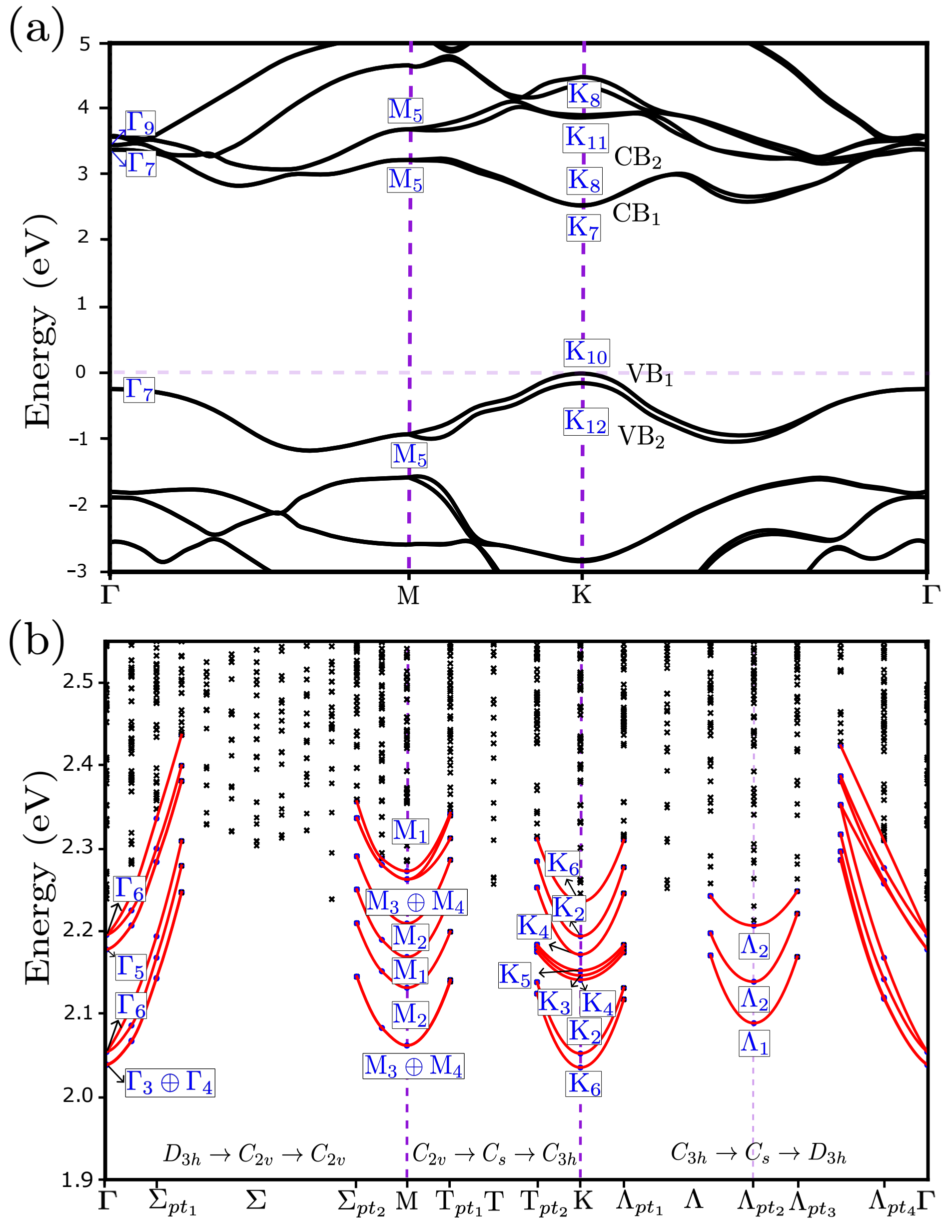

FIG. 1: (a) GW electronic band structure of monolayer MoS_2 along the high-symmetry path Γ-M-K-Γ in the Brillouin zone. The valence band maximum is set to 0 eV. The double-group spinor irreducible representations associated with the bands are indicated at the high-symmetry points. (b) Exciton band structure of monolayer MoS_2 along the path Γ-M-K-Γ in the Brillouin zone. The irreducible representations of the excitonic bands are labelled at the high-symmetry points Γ, M, and K. The irreducible representations at the labelled points along the high symmetry lines are tabulated in Table I. The evolution of the excitonic states at the transition between symmetry lines and high symmetry points illustrates the compatibility relations.

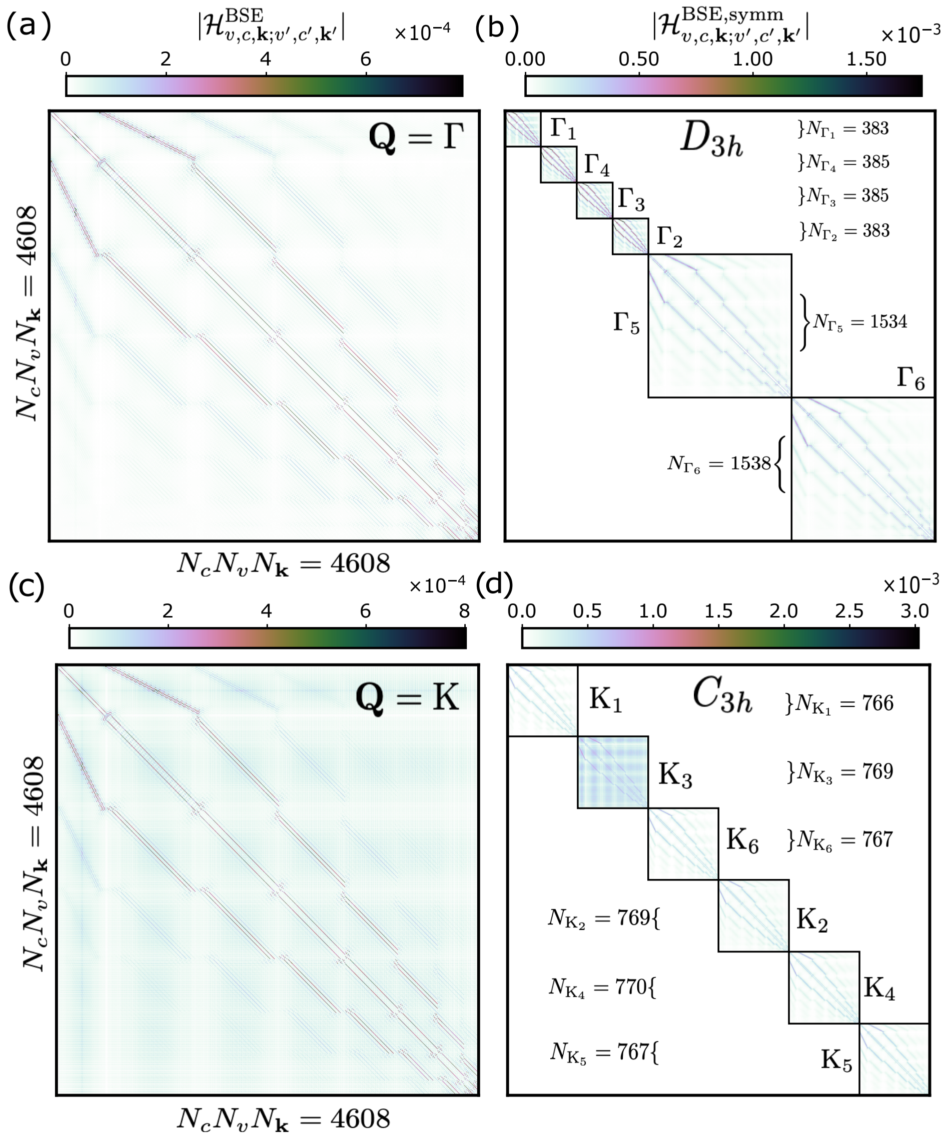

FIG. 2: (a) and (c) display the full spinor BSE Hamiltonian constructed from two valence and four conduction bands on a $24 \times 24 \times 1$ **k**-point grid, for exciton center-of-mass momenta $\mathbf{Q} = \Gamma$ and $\mathbf{Q} = \mathrm{K}$, respectively. Panels (b) and (d) show the corresponding block-diagonalized BSE Hamiltonians, resolved into blocks associated with the irreducible representations of the D_{3h} and C_{3h} symmetry groups at $\mathbf{Q} = \Gamma$ and $\mathbf{Q} = \mathrm{K}$, respectively. The dimensions of the blocks corresponding to each irreducible representation are indicated. The color bars represent the absolute values of the BSE Hamiltonian matrix elements for both the full and symmetry-adapted cases. For clarity, the diagonal matrix elements have been removed, and the color scale has been capped at a fixed maximum value to emphasize the block structure.

TABLE I: Irreducible representations of excitonic states at high-symmetry points and along high-symmetry lines in the Brillouin zone of monolayer MoS_2.

Symmetry line	Symmetry points	Symmetry Group	irreducible representations of the excitonic states
	Γ	D_{3h}	$\Gamma_3 \oplus \Gamma_4 \oplus \Gamma_6 \oplus \Gamma_5 \oplus \Gamma_6$
Σ	Σ_{pt_1}	C_{2v}	$\Sigma_3 \oplus \Sigma_4 \oplus \Sigma_2 \oplus \Sigma_1 \oplus \Sigma_3 \oplus \Sigma_4 \oplus \Sigma_2 \oplus \Sigma_1$
	Σ_{pt_2}	C_{2v}	$\Sigma_3 \oplus \Sigma_4 \oplus \Sigma_2 \oplus \Sigma_1 \oplus \Sigma_2 \oplus \Sigma_3 \oplus \Sigma_4 \oplus \Sigma_1$
	M	C_{2v}	$\mathrm{M}_3 \oplus \mathrm{M}_4 \oplus \mathrm{M}_2 \oplus \mathrm{M}_1 \oplus \mathrm{M}_2 \oplus \mathrm{M}_3 \oplus \mathrm{M}_4 \oplus \mathrm{M}_1$
T	T_{pt_1}	C_s	$\mathrm{T}_2 \oplus \mathrm{T}_2 \oplus \mathrm{T}_1 \oplus \mathrm{T}_1 \oplus \mathrm{T}_1 \oplus \mathrm{T}_2 \oplus \mathrm{T}_2 \oplus \mathrm{T}_2$
	T_{pt_2}	C_s	$\mathrm{T}_2 \oplus \mathrm{T}_1 \oplus \mathrm{T}_2 \oplus \mathrm{T}_1 \oplus \mathrm{T}_2 \oplus \mathrm{T}_2 \oplus \mathrm{T}_1 \oplus \mathrm{T}_1$
	K	C_{3h}	$\mathrm{K}_6 \oplus \mathrm{K}_2 \oplus \mathrm{K}_4 \oplus \mathrm{K}_3 \oplus \mathrm{K}_5 \oplus \mathrm{K}_4 \oplus \mathrm{K}_2 \oplus \mathrm{K}_6$
Λ	Λ_{pt_1}	C_s	$\Lambda_2 \oplus \Lambda_1 \oplus \Lambda_2 \oplus \Lambda_1 \oplus \Lambda_2 \oplus \Lambda_2 \oplus \Lambda_1 \oplus \Lambda_1$
	Λ_{pt_2}	C_s	$\Lambda_1 \oplus \Lambda_2 \oplus \Lambda_2 \oplus \Lambda_2 \oplus \Lambda_1 \oplus \Lambda_2 \oplus \Lambda_1 \oplus \Lambda_1$
	Λ_{pt_3}	C_s	$\Lambda_1 \oplus \Lambda_2 \oplus \Lambda_2 \oplus \Lambda_1 \oplus \Lambda_2 \oplus \Lambda_2 \oplus \Lambda_1 \oplus \Lambda_1$
	Λ_{pt_4}	C_s	$\Lambda_2 \oplus \Lambda_2 \oplus \Lambda_1 \oplus \Lambda_1 \oplus \Lambda_2 \oplus \Lambda_2 \oplus \Lambda_1 \oplus \Lambda_1$
	Γ	D_{3h}	$\Gamma_3 \oplus \Gamma_4 \oplus \Gamma_6 \oplus \Gamma_5 \oplus \Gamma_6$

calculating the irreducible representations of the little groups and classifying excitonic states accordingly, we demonstrated how symmetry governs their degeneracies and band connectivities. Moreover, using projection operators, we constructed symmetry-adapted linear combinations of electron–hole product states, which block-diagonalize the BSE Hamiltonian and provide a transparent symmetry classification of excitonic states. The irreducible representations of the excitonic states obtained with both the procedures were found to be in agreement with those derived from compatibility relations, confirming the consistency of the formalism. This unified approach highlights the central role of symmetry in excitonic theory and provides a robust framework for analyzing optical selection rules and exciton band connectivities in a broad class of quantum materials.

VI. ACKNOWLEDGEMENTS

We thank the Supercomputer Education and Research Centre (SERC) at the Indian Institute of Science (IISc) for providing the computational facilities. R.B. acknowledges the funding from the Prime Minister's Research Fellowship (PMRF), MHRD. M.J. and H.R.K. gratefully acknowledge the Nano mission of the Department of Science and Technology, India, and the Indian National Science Academy, India, for financial support under Grants No. DST/NM/TUE/QM-10/2019 and No. INSA/SP/SS/2023/, respectively.

APPENDIX A: TRANSLATIONAL SYMMETRY IN BETHE-SALPETER EQUATION (BSE) HAMILTONIAN

A1. BSE Hamiltonian in real space

We begin with the Bethe-Salpeter equation (BSE) for the electron-hole amplitude $\Psi(\mathbf{r}_e, \mathbf{r}_h)$, where $\mathbf{r}_e$ and $\mathbf{r}_h$ are the electron and hole coordinates, respectively. In real space, the BSE Hamiltonian acts as a four-point kernel:

$$\begin{aligned}
&\mathcal{H}_{\mathrm{BSE}}(\mathbf{r}_e, \mathbf{r}_h;\, \mathbf{r}'_e, \mathbf{r}'_h) = \mathcal{H}_e(\mathbf{r}_e, \mathbf{r}'_e)\, \delta(\mathbf{r}_h, \mathbf{r}'_h) \\
&+ \mathcal{H}_h(\mathbf{r}_h, \mathbf{r}'_h)\, \delta(\mathbf{r}_e - \mathbf{r}'_e) - \, W(\mathbf{r}_e, \mathbf{r}_h)\, \delta(\mathbf{r}_e - \mathbf{r}'_e)\, \delta(\mathbf{r}_h - \mathbf{r}'_h) \\
&+ \, v(\mathbf{r}_e, \mathbf{r}'_h)\, \delta(\mathbf{r}_e - \mathbf{r}_h)\, \delta(\mathbf{r}'_e - \mathbf{r}'_h)
\end{aligned} \tag{64}$$

where $\mathcal{H}_e(\mathbf{r}_e, \mathbf{r}'_e)$ and $\mathcal{H}_h(\mathbf{r}_h, \mathbf{r}'_h)$ are the electron quasiparticle and hole quasiparticle parts of Hamiltonian. $W(\mathbf{r}_e, \mathbf{r}_h)$ is the statically screened direct electron-hole interaction and $v(\mathbf{r}_e, \mathbf{r}'_h)$ is the bare Coulomb exchange term.

A2. Translational Invariance

In periodic crystals, the underlying crystal, ionic potentials, the coulomb interactions, quasiparticle self-energy (in the GW approximation), and screening are invariant under translations by any Bravais lattice vector $\mathbf{R}$. Also, the one-particle lattice translation operator, $\hat{T}^{e/h}_{\mathbf{R}}$ commutes the one-particle Hamiltonians, $\mathcal{H}_{e/h}(\mathbf{r}, \mathbf{r}')$. These properties leads to:

1. The electron and hole quasiparticle Hamiltonians are invariant with respect to discrete lattice translations:

$$\mathcal{H}_{e/h}(\mathbf{r}+\mathbf{R},\mathbf{r}'+\mathbf{R}) = \mathcal{H}_{e/h}(\mathbf{r},\mathbf{r}') \tag{65}$$

2. The interactions are invariant with respect to the discrete lattice translations as listed below:

$$\begin{aligned} W(\mathbf{r}+\mathbf{R},\mathbf{r}'+\mathbf{R}) &= W(\mathbf{r},\mathbf{r}') \\ v(\mathbf{r}+\mathbf{R},\mathbf{r}'+\mathbf{R}) &= v(\mathbf{r},\mathbf{r}') \end{aligned} \tag{66}$$

A3. BSE Kernel invariance under simultaneous translations

Translate all four coordinates by the same Bravais vector $\mathbf{R}$ as follows:

$$(\mathbf{r}_e,\mathbf{r}_h,\mathbf{r}'_e,\mathbf{r}'_h) \mapsto (\mathbf{r}_e+\mathbf{R},\mathbf{r}_h+\mathbf{R},\mathbf{r}'_e+\mathbf{R},\mathbf{r}'_h+\mathbf{R})$$

We examine each term in H.

$$\begin{aligned} &\mathcal{H}_e(\mathbf{r}_e+\mathbf{R},\mathbf{r}'_e+\mathbf{R})\,\delta(\mathbf{r}_h+\mathbf{R}-\mathbf{r}'_h-\mathbf{R}), \\ &=\mathcal{H}_e(\mathbf{r}_e,\mathbf{r}'_e)\,\delta(\mathbf{r}_h-\mathbf{r}'_h) \\ &\mathcal{H}_h(\mathbf{r}_h+\mathbf{R},\mathbf{r}'_h+\mathbf{R})\,\delta(\mathbf{r}_e+\mathbf{R}-\mathbf{r}'_e-\mathbf{R}), \\ &=\mathcal{H}_h(\mathbf{r}_h,\mathbf{r}'_h)\,\delta(\mathbf{r}_e-\mathbf{r}'_e), \\ &W(\mathbf{r}_e+\mathbf{R},\mathbf{r}_h+\mathbf{R})\,\delta(\mathbf{r}_e+\mathbf{R}-\mathbf{r}'_e-\mathbf{R})\,\delta(\mathbf{r}_h+\mathbf{R}-\mathbf{r}'_h-\mathbf{R}) \\ &=W(\mathbf{r}_e,\mathbf{r}_h)\,\delta(\mathbf{r}_e-\mathbf{r}'_e)\,\delta(\mathbf{r}_h-\mathbf{r}'_h), \\ &v(\mathbf{r}_e+\mathbf{R},\mathbf{r}'_h+\mathbf{R})\,\delta(\mathbf{r}_e+\mathbf{R}-\mathbf{r}_h+\mathbf{R})\,\delta(\mathbf{r}'_e+\mathbf{R}-\mathbf{r}'_h+\mathbf{R}) \\ &=v(\mathbf{r}_e,\mathbf{r}'_h)\,\delta(\mathbf{r}_e-\mathbf{r}_h)\,\delta(\mathbf{r}'_e-\mathbf{r}'_h). \end{aligned} \tag{67}$$

Each term reproduces its unshifted form, therefore

$$\mathcal{H}_{\mathrm{BSE}}(\mathbf{r}_e+\mathbf{R},\mathbf{r}_h+\mathbf{R};\,\mathbf{r}'_e+\mathbf{R},\mathbf{r}'_h+\mathbf{R}) = \mathcal{H}_{\mathrm{BSE}}(\mathbf{r}_e,\mathbf{r}_h;\,\mathbf{r}'_e,\mathbf{r}'_h) \tag{68}$$

This shows that the BSE Hamiltonian is invariant under simultaneous translations of all coordinates by any Bravais vector $\mathbf{R}$.

A4. Translation operator commutes with the Hamiltonian

Define the two-particle translation operator $\hat{T}^{ex}_{\mathbf{R}}$ acting on a two-particle function, $\Phi(\mathbf{r}_1, \mathbf{r}_2)$ as:

$$\left[\hat{T}^{ex}_{\mathbf{R}}\Phi\right](\mathbf{r}_1, \mathbf{r}_2) = \Phi(\mathbf{r}_1 - \mathbf{R}, \mathbf{r}_2 - \mathbf{R}) \tag{69}$$

Applying the BSE Hamiltonian to the translated amplitude gives:

$$\begin{aligned}
&\left[\hat{\mathcal{H}}_{\mathrm{BSE}}\,\hat{T}^{ex}_{\mathbf{R}}\Phi\right](\mathbf{r}_1, \mathbf{r}_2) \\
&= \iint d\mathbf{r}'_1 d\mathbf{r}'_2 \; \mathcal{H}_{\mathrm{BSE}}(\mathbf{r}_1, \mathbf{r}_2;\, \mathbf{r}'_1, \mathbf{r}'_2)\, \Phi(\mathbf{r}'_1 - \mathbf{R}, \mathbf{r}'_2 - \mathbf{R}). \\
&= \iint d\mathbf{r}'_1 d\mathbf{r}'_2 \; \mathcal{H}_{\mathrm{BSE}}(\mathbf{r}_1 - \mathbf{R}, \mathbf{r}_2 - \mathbf{R};\, \mathbf{r}'_1 - \mathbf{R}, \mathbf{r}'_2 - \mathbf{R}) \\
&\times \Phi(\mathbf{r}'_1 - \mathbf{R}, \mathbf{r}'_2 - \mathbf{R})
\end{aligned} \tag{70}$$

In the last equation, we have used the translational invariance of Hamiltonian. Changing integration variables to $\mathbf{r}''_1 = \mathbf{r}'_1 - \mathbf{R}$, $\mathbf{r}''_2 = \mathbf{r}'_2 - \mathbf{R}$, one finds:

$$\begin{aligned}
&\left[\hat{\mathcal{H}}_{\mathrm{BSE}}\,\hat{T}^{ex}_{\mathbf{R}}\Psi\right](\mathbf{r}_1, \mathbf{r}_2) \\
&= \iint d\mathbf{r}''_1 d\mathbf{r}''_2 \; \mathcal{H}_{\mathrm{BSE}}(\mathbf{r}_1 - \mathbf{R}, \mathbf{r}_2 - \mathbf{R};\, \mathbf{r}''_1, \mathbf{r}''_2)\, \Psi(\mathbf{r}''_1, \mathbf{r}''_2) \\
&= \iint d\mathbf{r}''_1 d\mathbf{r}''_2 \; \left[\hat{T}_{\mathbf{R}}\mathcal{H}_{\mathrm{BSE}}(\mathbf{r}_1, \mathbf{r}_2;\, \mathbf{r}''_1, \mathbf{r}''_2)\right]\, \Psi(\mathbf{r}''_1, \mathbf{r}''_2) \\
&= \left[\hat{T}^{ex}_{\mathbf{R}}\hat{\mathcal{H}}_{\mathrm{BSE}}\Psi\right](\mathbf{r}_1, \mathbf{r}_2)
\end{aligned} \tag{71}$$

This leads to:

$$\hat{\mathcal{H}}_{\mathrm{BSE}}\,\hat{T}^{ex}_{\mathbf{R}} = \hat{T}^{ex}_{\mathbf{R}}\,\hat{\mathcal{H}}_{\mathrm{BSE}}. \tag{72}$$

Therefore, $\hat{\mathcal{H}}_{\mathrm{BSE}}$ commutes with the two-particle translation operator.

A5. Bloch's Theorem for the Electron-Hole Amplitude

Since $\hat{\mathcal{H}}_{\mathrm{BSE}}$ commutes with $\hat{T}^{ex}_{\mathbf{R}}$, the electron-hole amplitudes are eigenfunctions of both $\hat{T}^{ex}_{\mathbf{R}}$ and $\mathcal{H}_{\mathrm{BSE}}$. Specifically,

$$\hat{T}^{ex}_{\mathbf{R}}\Psi_{S,\mathbf{Q}}(\mathbf{r}_e, \mathbf{r}_h) = e^{i\mathbf{Q}\cdot\mathbf{R}}\Psi_{S,\mathbf{Q}}(\mathbf{r}_e, \mathbf{r}_h) \tag{73}$$

where $\mathbf{Q}$ is the total momentum of the two-particle excitation state and S is the state index. Thus, translational invariance ensures that two-particle excitaions can be labeled by a well-defined crystal momentum $\mathbf{Q}$.

Now, we demonstrate the Bloch periodicity in the product state basis used in the main text. We begin from the electron-hole amplitude expansion of $\Psi_{S,\mathbf{Q}}(\mathbf{r}_e, \mathbf{r}_h)$ (Eq. 29) by simultaneously translating the electron and hole coordinates by $\mathbf{R}$ *i.e.* $\mathbf{r}_e \mapsto \mathbf{r}_e + \mathbf{R}$ and $\mathbf{r}_h \mapsto \mathbf{r}_h + \mathbf{R}$ which leaves the relative coordinate $\mathbf{r}$ unchanged and shifts the center-of-mass coordinate as $\mathbf{R}_{\text{cm}} \mapsto \mathbf{R}_{\text{cm}} + \mathbf{R}$. Using the single-particle Bloch's theorem and evaluating amplitude at the translated arguments gives:

$$
\begin{aligned}
&\Psi_{S,\mathbf{Q}}(\mathbf{r}_e + \mathbf{R}, \mathbf{r}_h + \mathbf{R}) \\
&= \sum_{v,c,\mathbf{k}} A^{S,\mathbf{Q}}_{v,c,\mathbf{k}} \, \Psi_{c,\mathbf{k}}(\mathbf{r}_e + \mathbf{R}) \, \Psi^*_{v,\mathbf{k}-\mathbf{Q}}(\mathbf{r}_h + \mathbf{R}) \\
&= \sum_{v,c,\mathbf{k}} A^{S,\mathbf{Q}}_{v,c,\mathbf{k}} \, e^{i\mathbf{k}\cdot\mathbf{R}} \Psi_{c,\mathbf{k}}(\mathbf{r}_e) \left(e^{i(\mathbf{k}-\mathbf{Q})\cdot\mathbf{R}} \Psi_{v,\mathbf{k}-\mathbf{Q}}(\mathbf{r}_h) \right)^* \\
&= e^{i\mathbf{Q}\cdot\mathbf{R}} \sum_{v,c,\mathbf{k}} A^{S,\mathbf{Q}}_{v,c,\mathbf{k}} \, \Psi_{c,\mathbf{k}}(\mathbf{r}_e) \, \Psi^*_{v,\mathbf{k}-\mathbf{Q}}(\mathbf{r}_h) \\
&= e^{i\mathbf{Q}\cdot\mathbf{R}} \, \Psi_{S,\mathbf{Q}}(\mathbf{r}_e, \mathbf{r}_h)
\end{aligned}
$$

In center-of-mass and relative coordinates this reads

$$
\Psi_{S,\mathbf{Q}}(\mathbf{R}_{\text{cm}} + \mathbf{R}, \mathbf{r}) = e^{\,i\mathbf{Q}\cdot\mathbf{R}} \, \Psi_{S,\mathbf{Q}}(\mathbf{R}_{\text{cm}}, \mathbf{r}) \tag{74}
$$

Define

$$
\mathbf{R}_{\text{cm}} = \alpha \, \mathbf{r}_e + \beta \, \mathbf{r}_h, \quad \mathbf{r} = \mathbf{r}_e - \mathbf{r}_h, \quad \alpha + \beta = 1
$$

so that $\mathbf{r}_e = \mathbf{R}_{\text{cm}} + \beta\mathbf{r}$, $\mathbf{r}_h = \mathbf{R}_{\text{cm}} - \alpha\mathbf{r}$, $\mathbf{k}_h = \mathbf{k} - \beta\mathbf{Q}$ and $\mathbf{k}_e = \mathbf{k} + \alpha\mathbf{Q}$

$$
\begin{aligned}
\Psi_{S,\mathbf{Q}}(\mathbf{R}_{\text{cm}}, \mathbf{r}) = e^{i\mathbf{Q}\cdot\mathbf{R}_{\text{cm}}} &\sum_{v,c,\mathbf{k}} A^{S,\mathbf{Q}}_{v,c,\mathbf{k}+\alpha\mathbf{Q}} \, e^{i\mathbf{k}\cdot\mathbf{r}} \\
&\times u_{c,\mathbf{k}+\alpha\mathbf{Q}}(\mathbf{R}_{\text{cm}} + \beta\mathbf{r}) \, u^*_{v,\mathbf{k}-\beta\mathbf{Q}}(\mathbf{R}_{\text{cm}} - \alpha\mathbf{r})
\end{aligned} \tag{75}
$$

Including normalization factors, the Bloch periodic form of the electron-hole amplitude can then be written as

$$
\Psi_{S,\mathbf{Q}}(\mathbf{R}_{\text{cm}}, \mathbf{r}) = \frac{1}{\sqrt{N_Q}} \, e^{i\mathbf{Q}\cdot\mathbf{R}_{\text{cm}}} F_{S,\mathbf{Q}}(\mathbf{R}_{\text{cm}}, \mathbf{r}) \tag{76}
$$

with the cell-periodic part

$$
F_{S,\mathbf{Q}}(\mathbf{R}_{\text{cm}}, \mathbf{r}) = \frac{1}{\sqrt{N_k}} \sum_{v,c,\mathbf{k}} A^{S,\mathbf{Q}}_{v,c,\mathbf{k}+\alpha\mathbf{Q}} \, e^{i\mathbf{k}\cdot\mathbf{r}} \tag{77}
$$

$$
\times \, u_{c,\mathbf{k}+\alpha\mathbf{Q}}(\mathbf{R}_{\text{cm}} + \beta\mathbf{r}) \, u^*_{v,\mathbf{k}-\beta\mathbf{Q}}(\mathbf{R}_{\text{cm}} - \alpha\mathbf{r}) \tag{78}
$$

Here, the cell-periodic part of two-particle excitation is lattice-periodic in the center-of-mass coordinate:

$$F_{S,\mathbf{Q}}(\mathbf{R}_{\text{cm}} + \mathbf{R}, \mathbf{r}) = F_{S,\mathbf{Q}}(\mathbf{R}_{\text{cm}}, \mathbf{r}).$$

For the symmetric case $\alpha = \beta = \frac{1}{2}$, the conduction and valence states carry momenta $\mathbf{k} + \frac{1}{2}\mathbf{Q}$ and $\mathbf{k} - \frac{1}{2}\mathbf{Q}$, respectively. For the calculation within BerkeleyGW, the form used in the Eq. 29 is used, which is $\alpha = 0$ and $\beta = 1$. The Bloch-periodic form expressed in these coordinates was previously discussed in Ref. [46] and is included here for completeness.

APPENDIX B: TRANSFORMATION OF EXCITONS UNDER TIME-REVERSAL SYMMETRY

Let Θ denote the time-reversal operator acting on the exciton amplitude $\Psi_{S,\mathbf{Q}}(\mathbf{r}_e, \mathbf{r}_h)$. Its action is defined as

$$\left(\hat{P}^{ex}_{\Theta}\Psi_{S,\mathbf{Q}}\right)(\mathbf{r}_e, \mathbf{r}_h) = \Psi^*_{S,\mathbf{Q}}(\mathbf{r}_e, \mathbf{r}_h) \tag{79}$$

where the complex conjugation acts on the coefficients and the single-particle spinor parts of the electron and hole wavefunctions. Since time-reversal reverses all crystal momenta, we have, at the single-particle operator level,

$$\hat{P}^{ex}_{\Theta}\, b^{\dagger}_{n,\mathbf{k},s}\, \hat{P}^{ex\,-1}_{\Theta} = \sum_{s'} (i\sigma_y)_{ss'}\; b^{\dagger}_{n,-\mathbf{k},s'} \tag{80}$$

and similarly for the hole creation operators; the same transformation is inherited by the exciton amplitude coefficients in the Bloch basis.

Using the translation property defined in Eqns. 69 and acting with $\hat{P}^{ex}_{\Theta}$ on the translated wavefunction gives:

$$\begin{aligned}\left[\hat{P}^{ex}_{\Theta}\,\hat{T}^{ex}_{\mathbf{R}}\Psi_{S,\mathbf{Q}}\right](\mathbf{r}_e, \mathbf{r}_h) &= \hat{P}^{ex}_{\Theta}\Big(\Psi_{S,\mathbf{Q}}(\mathbf{r}_e - \mathbf{R},\, \mathbf{r}_h - \mathbf{R})\Big) \\ &= \Psi^*_{S,\mathbf{Q}}(\mathbf{r}_e - \mathbf{R},\, \mathbf{r}_h - \mathbf{R})\end{aligned} \tag{81}$$

Because $\hat{P}^{ex}_{\Theta}$ is anti-unitary it complex-conjugates the phase factor, so applying it to the translation property defined in Eq. 73 yields

$$\begin{aligned}\left[\hat{P}^{ex}_{\Theta}\,\hat{T}^{ex}_{\mathbf{R}}\Psi_{S,\mathbf{Q}}\right](\mathbf{r}_e, \mathbf{r}_h) &= \left[\hat{P}^{ex}_{\Theta}\left(e^{i\mathbf{Q}\cdot\mathbf{R}}\Psi_{S,\mathbf{Q}}\right)\right](\mathbf{r}_e, \mathbf{r}_h) \\ &= e^{-i\mathbf{Q}\cdot\mathbf{R}}\left[\hat{P}^{ex}_{\Theta}\Psi_{S,\mathbf{Q}}\right](\mathbf{r}_e, \mathbf{r}_h)\end{aligned} \tag{82}$$

Compare this with the defining translation property similar to Eq. 73 for the amplitudes at $-\mathbf{Q}$:

$$\hat{T}^{ex}_{\mathbf{R}}\Psi_{S,-\mathbf{Q}}(\mathbf{r}_e,\mathbf{r}_h) = e^{-i\mathbf{Q}\cdot\mathbf{R}}\Psi_{S,-\mathbf{Q}}(\mathbf{r}_e,\mathbf{r}_h) \tag{83}$$

We therefore conclude that the time-reversed exciton amplitude $\left[\hat{P}^{ex}_{\Theta}\Psi_{S,\mathbf{Q}}\right](\mathbf{r}_e,\mathbf{r}_h)$ belongs to the momentum block $-\mathbf{Q}$ and using the fact that the time-reversal commutes with the BSE Hamiltonian, we get,

$$\hat{P}^{ex}_{\Theta}\,\mathcal{H}_{\mathbf{Q}}\,\hat{P}^{ex\,-1}_{\Theta} = \mathcal{H}_{-\mathbf{Q}} \tag{84}$$

If $\mathcal{H}_{\mathbf{Q}}\,\Psi_{S,\mathbf{Q}}(\mathbf{r}_e,\mathbf{r}_h) = \Omega_{S,\mathbf{Q}}\,\Psi_{S,\mathbf{Q}}(\mathbf{r}_e,\mathbf{r}_h)$, then applying $\hat{P}^{ex}_{\Theta}$ yields

$$\begin{aligned}\mathcal{H}_{-\mathbf{Q}}\,\left[\hat{P}^{ex}_{\Theta}\Psi_{S,\mathbf{Q}}\right](\mathbf{r}_e,\mathbf{r}_h) &= \left[\hat{P}^{ex}_{\Theta}\mathcal{H}_{\mathbf{Q}}\Psi_{S,\mathbf{Q}}\right](\mathbf{r}_e,\mathbf{r}_h)\\ &= \Omega_{S,\mathbf{Q}}\,\left[\hat{P}^{ex}_{\Theta}\Psi_{S,\mathbf{Q}}\right](\mathbf{r}_e,\mathbf{r}_h)\end{aligned} \tag{85}$$

Thus the time-reversed amplitude is an eigenfunction in the $-\mathbf{Q}$ block with the same eigenvalue:

$$\Omega_{S,\mathbf{Q}} = \Omega_{S,-\mathbf{Q}}, \qquad \left[\hat{P}^{ex}_{\Theta}\Psi_{S,\mathbf{Q}}\right](\mathbf{r}_e,\mathbf{r}_h) = \Psi_{S,-\mathbf{Q}}(\mathbf{r}_e,\mathbf{r}_h) \tag{86}$$

Equivalently, in Dirac notation,

$$\hat{P}^{ex}_{\Theta}\,|S,\mathbf{Q}\rangle = |S,-\mathbf{Q}\rangle\,, \tag{87}$$

which proves Eq. (34).

APPENDIX C: TRANSFORMATION OF EXCITONS UNDER SPACE GROUP SYMMETRIES

Consider a space group operation $\{\mathcal{R}_{\mathbf{t}}|\mathbf{t}\}$. Its action on the exciton amplitude is defined by:

$$\left(\hat{P}^{ex}_{\{\mathcal{R}_{\mathbf{t}}|\mathbf{t}\}}\Psi_{S,\mathbf{Q}}\right)(\mathbf{r}_e,\mathbf{r}_h) = \Psi({\mathcal{R}_{\mathbf{t}}}^{-1}(\mathbf{r}_e-\mathbf{t}),\,{\mathcal{R}_{\mathbf{t}}}^{-1}(\mathbf{r}_h-\mathbf{t}))$$

Firstly, we show that $\hat{P}^{ex}_{\{\mathcal{R}_{\mathbf{t}}|\mathbf{t}\}} \left|S, \mathbf{Q}\right\rangle$ belongs to the momentum block $\mathcal{R}_{\mathbf{t}}\mathbf{Q}$ We define the combined action of translations as defined in Eq. 69 along with space group operations as:

$$
\begin{aligned}
&\hat{P}^{ex}_{\{\mathcal{R}_{\mathbf{t}}|\mathbf{t}\}}\, \hat{T}^{ex}_{\mathbf{R}}\, (\hat{P}^{ex}_{\{\mathcal{R}_{\mathbf{t}}|\mathbf{t}\}})^{-1} \Psi_{S,\mathbf{Q}}(\mathbf{r}_e, \mathbf{r}_h) \\
&= \hat{T}^{ex}_{\mathbf{R}}\, (\hat{P}^{ex}_{\{\mathcal{R}_{\mathbf{t}}|\mathbf{t}\}})^{-1} \Psi_{S,\mathbf{Q}}(\mathcal{R}_{\mathbf{t}}{}^{-1}(\mathbf{r}_e - \mathbf{t}),\, \mathcal{R}_{\mathbf{t}}{}^{-1}(\mathbf{r}_h - \mathbf{t})) \\
&= \Psi_{S,\mathbf{Q}}\Big(\mathcal{R}_{\mathbf{t}}(\mathcal{R}_{\mathbf{t}}{}^{-1}(\mathbf{r}_e - \mathbf{t}) - \mathbf{R}) + \mathbf{t}, \\
&\mathcal{R}_{\mathbf{t}}(\mathcal{R}_{\mathbf{t}}{}^{-1}(\mathbf{r}_h - \mathbf{t}) - \mathbf{R}) + \mathbf{t} \Big) \\
&= \Psi_{S,\mathbf{Q}}(\mathbf{r}_e - \mathcal{R}_{\mathbf{t}}\mathbf{R},\, \mathbf{r}_h - \mathcal{R}_{\mathbf{t}}\mathbf{R}) = \left(\hat{T}^{ex}_{\mathcal{R}_{\mathbf{t}}\mathbf{R}} \Psi_{S,\mathbf{Q}} \right)(\mathbf{r}_e, \mathbf{r}_h)
\end{aligned}
$$

This gives the identity:

$$\hat{P}^{ex}_{\{\mathcal{R}_{\mathbf{t}}|\mathbf{t}\}}\, \hat{T}^{ex}_{\mathbf{R}}\, (\hat{P}^{ex}_{\{\mathcal{R}_{\mathbf{t}}|\mathbf{t}\}})^{-1} = \hat{T}^{ex}_{\mathcal{R}_{\mathbf{t}}\mathbf{R}}$$

Now, using the translation property defined in Eq. 73, we evaluate:

$$
\begin{aligned}
&\left(\hat{T}^{ex}_{\mathbf{R}} \hat{P}^{ex}_{\{\mathcal{R}_{\mathbf{t}}|\mathbf{t}\}} \Psi_{S,\mathbf{Q}} \right)(\mathbf{r}_e, \mathbf{r}_h) = \left(\hat{P}^{ex}_{\{\mathcal{R}_{\mathbf{t}}|\mathbf{t}\}} \hat{T}^{ex}_{\mathcal{R}_{\mathbf{t}}{}^{-1}\mathbf{R}} \Psi_{S,\mathbf{Q}} \right)(\mathbf{r}_e, \mathbf{r}_h) \\
&= e^{i\mathbf{Q}\cdot\mathcal{R}_{\mathbf{t}}{}^{-1}\mathbf{R}} \left(\hat{P}^{ex}_{\{\mathcal{R}_{\mathbf{t}}|\mathbf{t}\}} \Psi_{S,\mathbf{Q}} \right)(\mathbf{r}_e, \mathbf{r}_h) \\
&= e^{i(\mathcal{R}_{\mathbf{t}}\mathbf{Q})\cdot\mathbf{R}} \left(\hat{P}^{ex}_{\{\mathcal{R}_{\mathbf{t}}|\mathbf{t}\}} \Psi_{S,\mathbf{Q}} \right)(\mathbf{r}_e, \mathbf{r}_h)
\end{aligned}
$$

which implies that $\hat{P}^{ex}_{\{\mathcal{R}_{\mathbf{t}}|\mathbf{t}\}} \left|S, \mathbf{Q}\right\rangle$ lies in the momentum block labeled by $\mathcal{R}_{\mathbf{t}}\mathbf{Q}$. Also, the BSE Hamiltonian commutes with the symmetry operation. Therefore,

$$\mathcal{H}_{\mathcal{R}_{\mathbf{t}}\mathbf{Q}}\, \hat{P}^{ex}_{\{\mathcal{R}_{\mathbf{t}}|\mathbf{t}\}} = \hat{P}^{ex}_{\{\mathcal{R}_{\mathbf{t}}|\mathbf{t}\}}\, \mathcal{H}_{\mathbf{Q}}$$

If $\mathcal{H}_{\mathbf{Q}} \left|S, \mathbf{Q}\right\rangle = \Omega_{S,\mathbf{Q}} \left|S, \mathbf{Q}\right\rangle$, then

$$
\begin{aligned}
\left[\hat{P}^{ex}_{\{\mathcal{R}_{\mathbf{t}}|\mathbf{t}\}} \mathcal{H}_{\mathbf{Q}} \right] \left|S, \mathbf{Q}\right\rangle &= \Omega_{S,\mathbf{Q}} \left[\hat{P}^{ex}_{\{\mathcal{R}_{\mathbf{t}}|\mathbf{t}\}} \left|S, \mathbf{Q}\right\rangle \right] \\
\mathcal{H}_{\mathcal{R}_{\mathbf{t}}\mathbf{Q}} \left[\hat{P}^{ex}_{\{\mathcal{R}_{\mathbf{t}}|\mathbf{t}\}} \left|S, \mathbf{Q}\right\rangle \right] &= \Omega_{S,\mathbf{Q}} \left[\hat{P}^{ex}_{\{\mathcal{R}_{\mathbf{t}}|\mathbf{t}\}} \left|S, \mathbf{Q}\right\rangle \right]
\end{aligned} \tag{88}
$$

Hence, the rotated state $\hat{P}^{ex}_{\{\mathcal{R}_{\mathbf{t}}|\mathbf{t}\}} \left|S, \mathbf{Q}\right\rangle$ is an eigenstate of $\mathcal{R}_{\mathbf{t}}\mathbf{Q}$ momentum block of the Hamiltonian with the same eigenvalue. So, the following holds.

$$\Omega_{S,\mathcal{R}_{\mathbf{t}}\mathbf{Q}} = \Omega_{S,\mathbf{Q}}, \qquad \left|S, \mathcal{R}_{\mathbf{t}}\mathbf{Q}\right\rangle = \hat{P}^{ex}_{\{\mathcal{R}_{\mathbf{t}}|\mathbf{t}\}} \left|S, \mathbf{Q}\right\rangle$$

[1] E. Wigner, Gruppentheorie und ihre Anwendung auf die Quantenmechanik der Atomspektren, (1931).

[2] M. S. Dresselhaus, G. Dresselhaus, and A. Jorio, *Group Theory: Application to the Physics of Condensed Matter* (Springer, 2008).

[3] M. Tinkham, *Group Theory and Quantum Mechanics* (Dover Publications, 2003).

[4] G. F. Bassani and G. P. Parravicini, *Electronic States and Optical Transitions in Solids*, International Series of Monographs in the Science of the Solid State, Vol. 8 (Pergamon Press, 1975).

[5] Aroyo, Perez-Mato, Orobengoa, Tasci, D. L. Flor, and Kirov, Crystallography online: Bilbao crystallographic server, Bulgarian Chemical Communications **43**, 183 (2011).

[6] K. Shinohara, A. Togo, and I. Tanaka, spgrep: On-the-fly generator of space-group irreducible representations, Journal of Open Source Software **8**, 5269 (2023).

[7] M. Iraola, J. L. Mañes, B. Bradlyn, M. K. Horton, T. Neupert, M. G. Vergniory, and S. S. Tsirkin, Irrep: Symmetry eigenvalues and irreducible representations of ab initio band structures, Computer Physics Communications **272**, 108226 (2022).

[8] G. Onida, L. Reining, and A. Rubio, Electronic excitations: density-functional versus many-body Green's-function approaches, Rev. Mod. Phys. **74**, 601 (2002).

[9] M. Rohlfing and S. G. Louie, Electron-hole excitations and optical spectra from first principles, Phys. Rev. B **62**, 4927 (2000).

[10] S. Albrecht, L. Reining, R. Del Sole, and G. Onida, Ab initio Calculation of Excitonic Effects in the Optical Spectra of Semiconductors, Phys. Rev. Lett. **80**, 4510 (1998).

[11] M. Rohlfing and S. G. Louie, Electron-Hole Excitations in Semiconductors and Insulators, Phys. Rev. Lett. **81**, 2312 (1998).

[12] F. Wu, F. Qu, and A. H. MacDonald, Exciton band structure of monolayer MoS_2, Phys. Rev. B **91**, 075310 (2015).

[13] C. Robert, B. Han, P. Kapuscinski, A. Delhomme, C. Faugeras, T. Amand, M. R. Molas, M. Bartos, K. Watanabe, T. Taniguchi, B. Urbaszek, M. Potemski, and X. Marie, Measurement of the spin-forbidden dark excitons in MoS_2 and $MoSe_2$ monolayers, Nature Communications **11**, 4037 (2020).

[14] T. Galvani, F. Paleari, H. P. C. Miranda, A. Molina-Sánchez, L. Wirtz, S. Latil, H. Amara, and F. m. c. Ducastelle, Excitons in boron nitride single layer, Phys. Rev. B **94**, 125303 (2016).

[15] M. Zanfrognini, N. Spallanzani, M. Bonacci, E. Molinari, A. Ruini, M. J. Caldas, A. Ferretti, and D. Varsano, Effect of uniaxial strain on the excitonic properties of monolayer C_3n: A

symmetry-based analysis, Phys. Rev. B **107**, 045430 (2023).

[16] P. E. F. Junior, D. Hernangómez-Pérez, T. Amit, J. Fabian, and S. Refaely-Abramson, Generalized many-body exciton g-factors: magnetic hybridization and non-monotonic rydberg series in monolayer WSe_2 (2025), arXiv:2505.18468 [cond-mat.mes-hall].

[17] G. Kresse and J. Furthmüller, Efficient iterative schemes for ab initio total-energy calculations using a plane-wave basis set, Phys. Rev. B **54**, 11169 (1996).

[18] P. Giannozzi, S. Baroni, N. Bonini, M. Calandra, R. Car, C. Cavazzoni, D. Ceresoli, G. L. Chiarotti, M. Cococcioni, I. Dabo, A. Dal Corso, S. de Gironcoli, S. Fabris, G. Fratesi, R. Gebauer, U. Gerstmann, C. Gougoussis, A. Kokalj, M. Lazzeri, L. Martin-Samos, N. Marzari, F. Mauri, R. Mazzarello, S. Paolini, A. Pasquarello, L. Paulatto, C. Sbraccia, S. Scandolo, G. Sclauzero, A. P. Seitsonen, A. Smogunov, P. Umari, and R. M. Wentzcovitch, QUANTUM ESPRESSO: a modular and open-source software project for quantum simulations of materials, Journal of Physics: Condensed Matter **21**, 395502 (2009).

[19] X. Gonze, B. Amadon, P.-M. Anglade, J.-M. Beuken, F. Bottin, P. Boulanger, F. Bruneval, D. Caliste, R. Caracas, M. Côté, T. Deutsch, L. Genovese, P. Ghosez, M. Giantomassi, S. Goedecker, D. Hamann, P. Hermet, F. Jollet, G. Jomard, S. Leroux, M. Mancini, S. Mazevet, M. Oliveira, G. Onida, Y. Pouillon, T. Rangel, G.-M. Rignanese, D. Sangalli, R. Shaltaf, M. Torrent, M. Verstraete, G. Zerah, and J. Zwanziger, ABINIT: First-principles approach to material and nanosystem properties, Computer Physics Communications **180**, 2582 (2009).

[20] A. Togo and I. Tanaka, First principles phonon calculations in materials science, Scripta Materialia **108**, 1 (2015).

[21] A. Togo, First-principles Phonon Calculations with Phonopy and Phono3py, Journal of the Physical Society of Japan **92**, 012001 (2023).

[22] Y.-h. Chan, J. B. Haber, M. H. Naik, J. B. Neaton, D. Y. Qiu, F. H. da Jornada, and S. G. Louie, Exciton Lifetime and Optical Line Width Profile via Exciton-Phonon Interactions: Theory and First-Principles Calculations for Monolayer MoS_2, Nano Letters **23**, 3971 (2023).

[23] Y.-h. Chan, M. H. Naik, J. B. Haber, J. B. Neaton, S. G. Louie, D. Y. Qiu, and F. H. da Jornada, Exciton-Phonon Coupling Induces a New Pathway for Ultrafast Intralayer-to-Interlayer Exciton Transition and Interlayer Charge Transfer in WS_2-MoS_2 Heterostructure: A First-Principles Study, Nano Letters **24**, 7972 (2024).

[24] F. Paleari, H. P. C. Miranda, A. Molina-Sánchez, and L. Wirtz, Exciton-Phonon Coupling in the Ultraviolet Absorption and Emission Spectra of Bulk Hexagonal Boron Nitride, Phys. Rev. Lett. **122**, 187401 (2019).

[25] H.-Y. Chen, D. Sangalli, and M. Bernardi, Exciton-Phonon Interaction and Relaxation Times from First Principles, Phys. Rev. Lett. **125**, 107401 (2020).

[26] G. Antonius and S. G. Louie, Theory of exciton-phonon coupling, Phys. Rev. B **105**, 085111 (2022).

[27] M. Nalabothula, L. Wirtz, and S. Reichardt, Origin of Interlayer Exciton-Phonon Coupling in 2d Heterostructures, Nano Letters **25**, 6160 (2025).

[28] Y.-h. Chan, J. B. Haber, M. H. Naik, S. G. Louie, J. B. Neaton, F. H. da Jornada, and D. Y. Qiu, Exciton thermalization dynamics in monolayer MoS_2: A first-principles Boltzmann equation study, Phys. Rev. B **111**, 184305 (2025).

[29] D. Y. Qiu, F. H. da Jornada, and S. G. Louie, Optical spectrum of MoS_2: Many-body effects and diversity of exciton states, Phys. Rev. Lett. **111**, 216805 (2013).

[30] J. Noffsinger, E. Kioupakis, C. G. Van de Walle, S. G. Louie, and M. L. Cohen, Phonon-Assisted Optical Absorption in Silicon from First Principles, Phys. Rev. Lett. **108**, 167402 (2012).

[31] G. Marini, M. Calandra, and P. Cudazzo, Optical Absorption and Photoluminescence of Single-Layer Boron Nitride from a First-Principles Cumulant Approach, Nano Letters **24**, 6017 (2024).

[32] K. F. Mak, C. Lee, J. Hone, J. Shan, and T. F. Heinz, Atomically Thin MoS_2: A New Direct-Gap Semiconductor, Phys. Rev. Lett. **105**, 136805 (2010).

[33] G. G. Macfarlane, T. P. McLean, J. E. Quarrington, and V. Roberts, Fine Structure in the Absorption-Edge Spectrum of Si, Phys. Rev. **111**, 1245 (1958).

[34] G. Strinati, Dynamical Shift and Broadening of Core Excitons in Semiconductors, Phys. Rev. Lett. **49**, 1519 (1982).

[35] P. Giannozzi, O. Andreussi, T. Brumme, O. Bunau, M. Buongiorno Nardelli, M. Calandra, R. Car, C. Cavazzoni, D. Ceresoli, M. Cococcioni, N. Colonna, I. Carnimeo, A. Dal Corso, S. de Gironcoli, P. Delugas, R. A. DiStasio, A. Ferretti, A. Floris, G. Fratesi, G. Fugallo, R. Gebauer, U. Gerstmann, F. Giustino, T. Gorni, J. Jia, M. Kawamura, H.-Y. Ko, A. Kokalj, E. Küçükbenli, M. Lazzeri, M. Marsili, N. Marzari, F. Mauri, N. L. Nguyen, H.-V. Nguyen,

A. Otero-de-la Roza, L. Paulatto, S. Poncé, D. Rocca, R. Sabatini, B. Santra, M. Schlipf, A. P. Seitsonen, A. Smogunov, I. Timrov, T. Thonhauser, P. Umari, N. Vast, X. Wu, and S. Baroni, Advanced capabilities for materials modelling with Quantum ESPRESSO, Journal of Physics: Condensed Matter **29**, 465901 (2017).

[36] J. P. Perdew, K. Burke, and M. Ernzerhof, Generalized Gradient Approximation Made Simple, Phys. Rev. Lett. **77**, 3865 (1996).

[37] D. R. Hamann, Optimized norm-conserving Vanderbilt pseudopotentials, Phys. Rev. B **88**, 085117 (2013).

[38] M. van Setten, M. Giantomassi, E. Bousquet, M. Verstraete, D. Hamann, X. Gonze, and G.-M. Rignanese, The PseudoDojo: Training and grading a 85 element optimized norm-conserving pseudopotential table, Computer Physics Communications **226**, 39 (2018).

[39] M. S. Hybertsen and S. G. Louie, Electron correlation in semiconductors and insulators: Band gaps and quasiparticle energies, Phys. Rev. B **34**, 5390 (1986).

[40] J. Deslippe, G. Samsonidze, D. A. Strubbe, M. Jain, M. L. Cohen, and S. G. Louie, BerkeleyGW: A massively parallel computer package for the calculation of the quasiparticle and optical properties of materials and nanostructures, Computer Physics Communications **183**, 1269 (2012).

[41] B. A. Barker, J. Deslippe, J. Lischner, M. Jain, O. V. Yazyev, D. A. Strubbe, and S. G. Louie, Spinor GW/Bethe-Salpeter calculations in BerkeleyGW: Implementation, symmetries, benchmarking, and performance, Phys. Rev. B **106**, 115127 (2022).

[42] F. H. da Jornada, D. Y. Qiu, and S. G. Louie, Nonuniform sampling schemes of the Brillouin zone for many-electron perturbation-theory calculations in reduced dimensionality, Phys. Rev. B **95**, 035109 (2017).

[43] S. Ismail-Beigi, Truncation of periodic image interactions for confined systems, Phys. Rev. B **73**, 233103 (2006).

[44] G. F. Koster, J. O. Dimmock, R. G. Wheeler, and H. Statz, *Properties of the Thirty-Two Point Groups*, Vol. 24 (MIT Press, 1963).

[45] D. Y. Qiu, T. Cao, and S. G. Louie, Nonanalyticity, Valley Quantum Phases, and Lightlike Exciton Dispersion in Monolayer Transition Metal Dichalcogenides: Theory and First-Principles Calculations, Phys. Rev. Lett. **115**, 176801 (2015).

[46] J. B. Haber, D. Y. Qiu, F. H. da Jornada, and J. B. Neaton, Maximally localized exciton

Wannier functions for solids, Phys. Rev. B **108**, 125118 (2023).

[47] A. Marini, C. Hogan, M. Grüning, and D. Varsano, yambo: An ab initio tool for excited state calculations, Computer Physics Communications **180**, 1392 (2009).

[48] A. Chernikov, T. C. Berkelbach, H. M. Hill, A. Rigosi, Y. Li, B. Aslan, D. R. Reichman, M. S. Hybertsen, and T. F. Heinz, Exciton Binding Energy and Nonhydrogenic Rydberg Series in Monolayer WS_2, Phys. Rev. Lett. **113**, 076802 (2014).

[49] Y. Li, A. Chernikov, X. Zhang, A. Rigosi, H. M. Hill, A. M. van der Zande, D. A. Chenet, E.-M. Shih, J. Hone, and T. F. Heinz, Measurement of the optical dielectric function of monolayer transition-metal dichalcogenides: MoS_2, $MoSe_2$, WS_2, and WSe_2, Phys. Rev. B **90**, 205422 (2014).

[50] W. Kohn and L. J. Sham, Self-Consistent Equations Including Exchange and Correlation Effects, Phys. Rev. **140**, A1133 (1965).